UNIVERSITÀ DEGLI STUDI DI PADOVA

UNIVERSITA' DEGLI STUDI DI PADOVA

**Dipartimento di Ingegneria Industriale DII**

Corso di Laurea Magistrale in Materials Engineering

# *MECHANICAL AND ELASTOCALORIC PROPERTIES OF NATURAL RUBBER / DEVULCANIZED WASTE RUBBER BLENDS*

Relatore interno: Prof. Alessandro Martucci

Relatore esterno: Prof. Nicolas Candau

Studente: Samuele Uliana con matricola 2095774

Anno Accademico 2023/2024

# Abstract

Nowadays, one of the biggest challenges in polymer industry is to find new roots for the recovery and the recycling of the plastic waste, and particularly the exhausted tyres. In this work the Ground Tire Rubber (GTR) is used as a filler for the preparation of blends with Natural Rubber (NR) matrix. In the first part of the work GTR is added to the NR without devulcanization process, with 10-20-33-40 phr, vulcanizing the blend with dicumyl peroxide (DCP). The effect of Strain Induced crystallization (SIC) on the mechanical properties of NR/GTR blends is evaluated qualitatively thanks to the diffraction images obtained during in-situ WAXS measurements performed with synchrotron radiation. SEM microscopy is used to evaluate the fracture mechanism of these blends. In the second part, GTR particles with size of 63 μm < d <100 μm are devulcanized with microwave radiation with different set of Powers: 80,400,640,800 W and times: 1,2,3,5,10 minutes. The devulcanized particles are then characterized by swelling tests, thermogravimetric analysis (TGA) and FTIR spectroscopy. The devulcanized GTR (GTRD) with 800 W is finally used to prepare NR/GTRD blends with 20 phr, vulcanized with sulphur, and the effect of the devulcanization time on the elastocaloric properties is analysed.

# Appreciations

This thesis work is one of the best projects and opportunities that I had during my entire academic career. For this reason, I want firstly to thanks e-Plascom group to allowing me to make research on their eco-friendly materials, as it is a fundamental aspect for the development of renewable technologies, which I care a lot about.

I want to thank my supervisor Nicolas Candau, who constantly supported and helped me during all my stay, stimulating my work and giving me the possibility to perform different kinds of experiments which I never had the opportunity to make, increasing my experience and my knowledge in this field.

Thanks to prof. Alessandro Martucci who gave me his availability and allowed me to work at Universitat Politécnica de Catalunya.

Finally, I want to say thanks to the most important people in my life: my parents, my best friends and my family who always supported me constantly during my academic career and during all my life, giving me advice and stimulating me to catch all the opportunities that the world present to me.

# Glossary

| | |
|---|---|
| **CB** | Carbon Black |
| **CNT** | Carbon nanotubes |
| **eC** | Elastocaloric |
| **MR** | Mooney Rivlin |
| **NR** | Natural Rubber |
| **GTR** | Ground Tire Rubber |
| **GTRD** | Devulcanized Ground Tire Rubber |
| **rpm** | Round per minute |
| **SIC** | Strain Induced Crystallization |
| **TIC** | Temperature Induced Crystallization |
| **%wt.** | Weight percentage |
| | |
| **A** | Amplification factor |
| **C** | Heat Capacity |
| **E** | Young's Modulus |
| **$E_m$** | Mechanical Energy |
| **d** | Particle size |
| **ε** | Engineering strain |
| **F** | Force, Helmholtz Free Energy |
| **f** | Network functionality |
| **ψ** | Functionality parameter |
| **φ** | Filler volume fraction |
| **k** | Boltzmann constant, thermal conductivity |
| **λ** | Stretching ratio |
| **m** | Mass |
| **N** | Number of statistical elements |
| **n** | Number of chains |
| **l** | Displacement |
| **Ω** | Thermodynamic potential |
| **ρ** | Weight density |
| **R** | Gas constant |
| **Q** | Swelling ratio, Heat exchanged |
| **$\sigma_{exp}$** | Engineering stress |
| **$\sigma_{MR}$** | Mooney-Rivlin stress |
| **S** | Entropy of deformation |
| **s** | Solubility |
| **T** | Temperature |
| **t** | Time, thickness |
| **v** | Network Chain Density |
| **$W_{gap}$** | Strain energy difference |
| **w** | Width |
| **ω** | Distribution function |
| **χ** | Crystallinity, Flory-Huggin's parameter |

# Table of Figures

*Figure 1 1,4 cis-polyisoprene[1].* 14

*Figure 2 Crosslinks scheme for natural rubber[4].* 15

*Figure 3 Crosslinking of polyisoprene with peroxides[6].* 15

*Figure 4 On the left, stress-strain curves for different type of polymers. On the right stress-strain curves dependence on temperature[9].* 16

*Figure 5 SEM of NR/NBR/devulcanized GTR composites at fracture[11]* 17

*Figure 6 SEM of NR filled with 150 phr of N772 CB[13].* 18

*Figure 7 Schematization of SIC[18]* 20

*Figure 8 Stress relaxation in natural rubber[17].* 21

Figure 9 On the left: Representation on the 3 main stages leading to SIC. On the right: stress-strain curves related to the thermodynamic description by Flory. 22

*Figure 10 Example of diffraction pattern for natural rubber[22].* 24

*Figure 11 Elastocaloric effect during loading/unloading of NR[24].* 25

*Figure 12 Energy of the bonds involved during devulcanization process.* 27

*Figure 13 GTR reactions induced by heating.* 28

*Figure 14 Parameters influencing the thermal conductivity of NR composites.* 30

*Figure 15 Examples of CB interconnected aggregates (TEM[34]).* 31

*Figure 16 a) Pristine CNTs b)CNTs functionalized with CB[36].* 32

*Figure 17 SMR Natural Rubber.* 33

*Figure 18 Ground Tire Rubber particles.* 33

*Figure 19 Sifters for 63 µm and 100 µm sieving.* 34

*Figure 20 Microwave apparatus for devulcanization.* 35

*Figure 21 On the left, contact digital thermometer (HANNA). On the right, laser digital thermometer (Raytek).* 36

*Figure 22 Vulcanizing agents and additives.* 37

*Figure 23 Internal mixer for blending (BRABENDER).* 38

*Figure 24 NR/GTRD blend.* 38

*Figure 25 Hot press for molding and vulcanization.* 39

*Figure 26 Stamping machine and NR/GTRD sample.* 40

*Figure 27 Schematization of the beamline BL11-NCD-SWEET of ALBA synchrotron.* 41

*Figure 28 Stretcher - TST350 for uniaxial tensile tests.* 42

*Figure 29 INSIZE Micrometer for thickness measurements.* 42

*Figure 30 Example of FTIR spectrum of devulcanized GTR.* 44

*Figure 31 Samples for swelling test of GTR devulcanized powder.* 46

*Figure 32 Machine and gas regulation system for TGA.* 47

*Figure 33 Example of TGA test performed for GTRD with 640W.* 47

*Figure 34 On the left the tensile testing machine. On the right the IR camera.* 48

*Figure 35 Evolution of the temperature of the samples with IR camera.* 49

*Figure 36 fe-SEM machine and desktops.* 49

*Figure 37 Coating process with sputtering.* 50

*Figure 38 a) Cross link density of NR/GTRx samples b) Soluble fraction of NR/GTRx samples.* 51

*Figure 39 Experimental and Mooney-Rivlin stress-strain curves for different NR/GTRx composites.* 53

*Figure 40 Young's Modulus of NR/GTRx composites evaluated with MR model.* 54

*Figure 41 a) Difference in strain energy between Experimental and MR model for NR/GTRx b) Onset of crystallization for NR/GTRx.* 55

*Figure 42 Comparison between cross link densities, evaluated with MR constants and swelling experiments.* _____ 56

*Figure 43 Stress-strain curves at Tamb and V2=10 mm/min for different compositions.* _____ 57

*Figure 44 a) Top: Stress strain curve for NR/GTR10 at different strain rates. Bottom: Diffraction patterns of NR/GTR10 at V1 and V3. b) Top: Stress-strain curve for NR/GTR20 at different strain rates. Bottom: Diffraction patterns of NR/GTR20 at V1 and V2.* _____ 58

*Figure 45 Stress strain curves at different temperatures for a) NR b) NR/GTR10 c) NR/GTR20.* __ 59

*Figure 46 Top: Stress-strain curves for NR, NR/GTR10, NR/GTR20 at different temperatures (a-d). Bottom: Diffraction patterns taken at fracture point.*_____ 60

*Figure 47 a) Cyclic curves for NR/GTRx at V2=10 mm/min b) Energy dissipated in hysteresis for different compositions.* _____ 61

*Figure 48 3D Loading and thermal cycle: Stretching, Heating, Cooling, De-stretching.* _____ 62

*Figure 49 Up: a) Fracture temperature at different composition during heating at fixed deformation. Bottom: Diffraction images at different temperature until fracture.* _____ 63

*Figure 50 SEM images of the fracture surfaces of NR/GTR samples. Up: 25X magnification Bottom:300X magnification.*_____ 64

*Figure 51 SEM images of NR/GTR at 1000X magnification.*_____ 65

*Figure 52 SEM image of NR/GTR40 at 10000X magnification.* _____ 66

*Figure 53 TGA curves for GTRD at different powers: a) 80W b) 400W c) 640W d) 800W* _____ 67

*Figure 54 CB content of GTRD at different powers.* _____ 68

*Figure 55 Cross-link density as function of devulcanization time for different powers.* _____ 69

*Figure 56 Temperature of the samples after devulcanization.*_____ 70

*Figure 57 Ratio of the bonds evaluated from FTIR spectroscopy.* _____ 71

*Figure 58 Tensile tests for NR/GTRD800: a) Stress-strain curve b) Difference in temperature respect the deformation c) Stress at fracture respect devulcanization time d) Maximum difference in temperature respect devulcanization time* _____ 73

*Figure 59 Cyclic tests for NR/GTRD800: a) Stress-strain curves b) Difference in temperature respect deformation.* _____ 74

*Figure 60 Cyclic test for NR/GTRD800: a) Maximum difference in temperature during heating b) Maximum difference in temperature during cooling c) Maximum difference in temperature during the entire cycle d) Mechanical energy dissipated during the entire cycle* _____ 75

*Figure 61 COP of NR/GTRD800 at different devulcanization times.*_____ 76

## List of tables

*Table 1 Nomenclature of devulcanized GTR* _____ 36

*Table 2 Composition of NR/GTRD800 blends*_____ 39

# INDEX

**ABSTRACT** ____ **3**

**APPRECIATIONS** ____ **4**

**GLOSSARY** ____ **5**

**TABLE OF FIGURES** ____ **6**

**1. INTRODUCTION** ____ **13**

**1.1. Objective** ..... 13

**1.2. Scope** ..... 13

**2. THEORETICAL FRAMEWORK** ____ **14**

**2.1. Natural Rubber (NR)** ..... 14

**2.1.1. Chemical and structural composition** ..... 14

**2.1.2. Vulcanization processes** ..... 14

**2.1.3. Mechanical behaviour** ..... 15

**2.1.4. Fracture behaviour of filled NR** ..... 16

**2.1.5. Models for NR tensile curves** ..... 18

**2.2. Strain Induced Crystallization (SIC) and Elastocaloric effect (eC)** ..... 20

**2.2.1. Crystallization in natural rubbers** ..... 20

**2.2.2. Flory's theory and thermodynamic of SIC** ..... 21

**2.2.3. Effect of fillers in SIC** ..... 23

**2.2.4. X-ray diffraction for studying crystalline structures.** ..... 23

**2.2.5. Elastocaloric effect of NR** ..... 25

**2.3. Ground Tires Rubber (GTR)** ..... 26

**2.3.1. Recycling of GTR** ..... 26

**2.3.2. Devulcanization of GTR** ..... 26

**2.4. Thermally Conductive Fillers for Natural Rubber** ..... 28

**2.4.1. Improvement of NR thermal conductivity** ..... 28

**2.4.2. Carbon based conductive fillers** ..... 30

**3. MATERIALS PREPARATION** ____ **33**

**3.1. Natural Rubber (NR)** ..... 33

**3.2. Ground Tire Rubber (GTR)** ..... 33

**3.2.1. Raw materials** ..... 33

**3.2.2. Sieving** ..... 34

**3.2.3. Microwave devulcanization** ..... 34

3.3. Vulcanizing agents and Additives ..... 37
3.4. Internal mixing ..... 38
3.5. Compression Molding and Hot pressing ..... 39
3.6. Stamping ..... 40

4. EXPERIMENTS ..... 41
4.1. In situ WAXS and mechanical tests at synchrotron ALBA ..... 41
4.2. FTIR spectroscopy ..... 44
4.3. Swelling ..... 45
4.4. Thermogravimetric Analysis (TGA) ..... 46
4.5. Mechanical tests with Infrared Camera ..... 48
4.6. Field Emission Scanning Electron Microscope (fe-SEM) ..... 49

5. RESULTS AND DISCUSSION ..... 51
5.1. NR/GTR composites characterization ..... 51
5.1.1. Swelling of NR/GTR ..... 51
5.1.2. Mooney-Rivlin model for tensile tests and strain induced crystallization. ..... 52
5.1.3. Tensile tests: Effect of GTR content ..... 56
5.1.4. Tensile tests: Effect of strain rate ..... 57
5.1.5. Tensile tests: Effect of temperature ..... 58
5.1.6. Cyclic tests: Hysteresis ..... 60
5.1.7. Cyclic tests: Thermal cycles ..... 61
5.1.8. Cyclic tests: Fracture of NR/GTR during thermal cycles ..... 62
5.1.9. Fracture analysis of NR/GTR with SEM. ..... 63
5.2. Devulcanization of GTR particles ..... 66
5.2.1. TGA of GTRs ..... 66
5.2.2. Swelling of GTR particles ..... 68
5.2.3. Temperature of the devulcanized GTR particles ..... 70
5.2.4. FTIR spectroscopy ..... 71
5.3. Elastocaloric properties of NR/GTRD blends ..... 72
5.3.1. Tensile tests on NR/GTRD800 blends ..... 72
5.3.2. Cyclic tests of NR/GTRD800 blends ..... 73
5.3.3. Coefficient of performance of NR/GTRD800 blends ..... 76

CONCLUSIONS ..... 78

BIBLIOGRAPHY ..... 79

# 1. Introduction

## 1.1. Objective

The general objective of this work is to design natural rubber-based blends for heating/cooling applications, using ground tyre rubber (GTR) to optimize the strain induced crystallization (SIC) and elastocaloric (eC) effect.

From the experimental point of view, the first specific objective is to characterize the mechanical properties of NR/GTR blends with different amount of GTR, which are tested in different conditions of temperature and strain rate to observe the influence of the filler's quantity in SIC, thanks to in-situ WAXS measurements performed at ALBA's synchrotron.

The second specific objective is to perform devulcanization with microwave of the GTR powder with different set of power and times to observe the effect in the composition of this process, particularly the presence of carbon black, the reinforcing agent in the GTR. The devulcanized GTR (GTRD) is characterized using different techniques as TGA, FTIR spectroscopy and swelling tests.

The third specific objective is to prepare NR/GTRD blends and observe their elastocaloric properties performing mechanical tests with the utilization of IR thermography technique.

## 1.2. Scope

The main goals of this study are to firstly understand the influence of the amount of GTR filler in the mechanical properties of the pure NR rubber and secondly to understand the effectiveness of the devulcanization process of GTR particles. Both parts are strictly related with the elastocaloric properties of the material, which are the one responsible for the ability of the material to undergo heating and cooling cycles.

SIC is firstly studied as it directly influences the elastocaloric effect, and particularly the amount of heat that can be released or absorbed by the material during mechanical cycles. Then, the devulcanization process has been performed to improve the processing of the NR/GTRD blends trough the building of the interface between the NR and GTR during their re-vulcanization. Finally, the effect of the devulcanization on the mechanical stableness and the elastocaloric properties of these blends has been studied.

# 2. Theoretical Framework

## 2.1. Natural Rubber (NR)

### 2.1.1. Chemical and structural composition

The most important source of natural rubber is the tree of *Hevea brasiliensis*, which contains a milky fluid from which is possible to extract about 35% of natural rubber, dispersed in the form of particles. Rubber is composed of polymeric chains of 1,4 cis-polyisoprene (Figure 1), with an average degree of polymerization of 3,000–5,000, and by other non-isoprene groups, which are classified as fatty acids, phospholipids, and proteins.

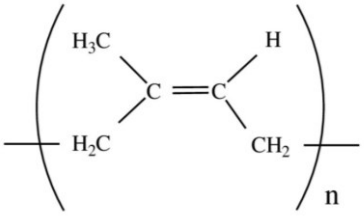


*Figure 1 1,4 cis-polyisoprene[1].*

These groups, even if present in low concentration, ensure higher mechanical properties with respect to the synthetic rubbers made only by 1,4 cis-polyisoprene and synthesized with Zieglar-Natta catalysts. That's why natural rubber is still occupying around 40% of the market of all the rubbers[2,3].

### 2.1.2. Vulcanization processes

The natural rubber is very soft and sticky material, with 50-70% of gel phase, and it needs to be vulcanized to achieve higher strength and resistance to deformation. The vulcanization is a process that allows the formation of intermolecular covalent bonds between the polymeric chains, which are also called chemical crosslinks, through different chemical reactions, resulting in a three-dimensional network structure (Figure 2).

The most common and traditional way is the sulphur vulcanization, which mixes the rubber with sulphur compounds, allowing the formation of sulphur bridges between the polymeric chains in correspondence of the unsaturation points of the rubber (C=C bonds). The sulphur cross links possible are three: C-S-C, C-$S_2$-C, and C-$S_X$--C. Depending on the level of rigidity needed and the type of application, the sulphur compound can vary between 1-10% in weight of the final material.

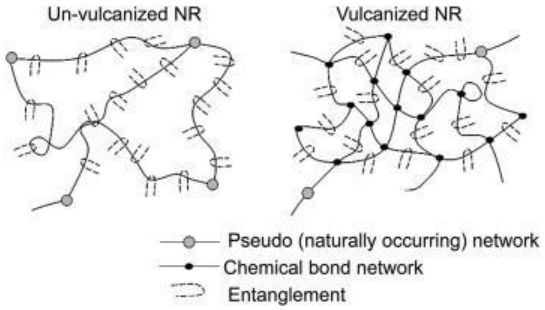


*Figure 2 Crosslinks scheme for natural rubber[4].*

Another possibility for the vulcanization is to make it through peroxides. The advantage of the peroxides, with respect to the sulphur, is that they are also able to cross-link unsaturated polymers, such as LDPE and EPR through radical reactions (Figure 3). Another advantage is the simplicity of the process, and the short time needed. The main disadvantages are the high cost of the crosslinker's agents and the possibility to have secondary radical reactions, for example with antioxidants[5]. One of the most common peroxides used is the dicumyl peroxide DCP, used in small amounts, between 1-5 phr[6].

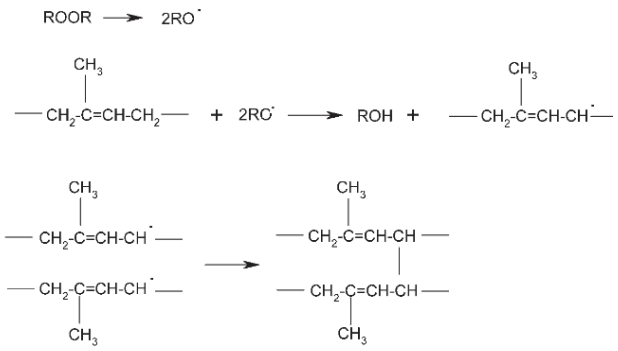


*Figure 3 Crosslinking of polyisoprene with peroxides[6].*

### 2.1.3. Mechanical behaviour

The natural rubber mechanical behaviour is referred as elastomeric, or better viscoelastic, as the rubber can deform both elastically, thanks to the crosslinks, and in a viscous way, through the sliding of the polymer chains. From the mechanical point of view, the viscoelastic character is modelled through combinations of springs, for the elastic part, which follows the Hooke's law and pistons, for the viscous part, which follow Newton's laws[7]. The mechanical response has strong dependence on the loading conditions, in particular the strain rate, and the temperature (Figure 4). At higher strain rate the rubber will tend to behave with an elastic behaviour, as the polymer chains don't have time to slide, and the stress-strain curve will be more like the ones related to fragile materials. A rigid

response is given also, when the operative temperature is near or below the glass transition temperature Tg mainly due to the reduction of the free volume for the relative movement of the chains. On the contrary, at lower strain rate, the chains have time to slide in a viscous way reaching much higher deformation and behaving in a rubber-like way. This is the expected behaviour of the rubber at ambient temperature, which is much higher than the Tg=-60°C. When reaching high deformation, which can arrive up to 1000%, the failure occurs, first with creation of microcavities and then with their growth until the formation of the crack and the consecutive rupture of the material[8]. This mechanism requires more external energy, those increasing the toughness of the material. The different mechanical responses ensure the possibility of using this material, both for mechanical structures and mostly as energy absorbers and vibration dampers, thanks to the viscous dissipation.

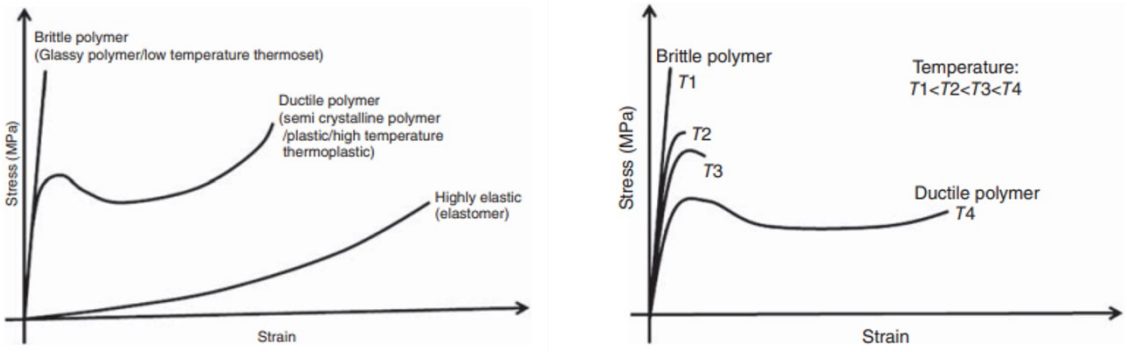


*Figure 4 On the left, stress-strain curves for different type of polymers. On the right stress-strain curves dependence on temperature[9].*

### 2.1.4. Fracture behaviour of filled NR

When filled NR is stretched with a tensile force, the most common mechanism of failure of these materials is cracking, which can be divided in two main steps: initiation and crack growth or propagation. The strength of the material and the ability to avoid fracture are directly related to its energy dissipation capability. For pure NR the energy is mainly dissipated by the breakage of the polymeric chains of the network which, after failure, transfer the load to the surrounding chains that will break quickly in a cascade process, leading to a catastrophic macro-crack initiation and propagation. The vulcanization of the rubber increases the strength of the NR, as some energy can be dissipated by internal friction and network rearrangement. Another mechanism for NR is micro-cavitation, with the formation of voids and fibrils.

When a rigid inclusion, as CB, is added to a soft matrix, during loading there will be an increase of the stress near the inclusion, those causing possible crack initiation. However, the dimensions of the inclusions and their distribution plays a fundamental role. Even if fillers accelerate crack initiation

process, they can have positive effect, as if present in enough quantity in the matrix, they can avoid crack propagation acting as obstacle and deviating the path of the crack. If the particles are enough smaller (d ≤1 μm), the splitting of the main crack in 2 new cracks which will then propagate in 2 opposite directions can happen. On the other way, if the quantity of filler is not enough, cracks will have enough space to propagate in the unhindered NR matrix, leading to a quick fracture[10].

A fundamental aspect that influences the crack initiation is the strength of the interface between the filler and the matrix. The starting of the crack in proximity of the rigid particles is due to a poor adhesion of the filler, which can be seen by the consequential formation of large voids around the particles as shown in Figure 5. The largest particles manifest highly this phenomenon due to a smaller specific surface area compared to the smaller particles. In NR/GTR blends the interface between GTR and NR can be improved by the devulcanization process[11], which will be analysed in the next section.

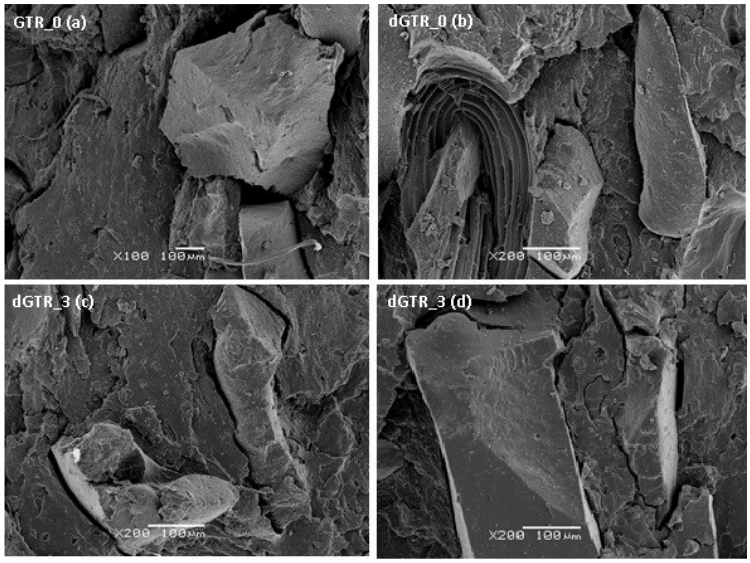


*Figure 5 SEM of NR/NBR/devulcanized GTR composites at fracture[11]*

Before the cracking, the concentration of the stress near the particle causes an alignment of the chains along the stretching direction. As crack growth happen mainly in the perpendicular direction respect the stretching one, the alignment of the chain and the strain induced crystals will inhibit the lateral expansion of the crack. As shown in Figure 6, the high alignment of the chains can be observed by the formation of fibrils along the stretching direction , with a diameter that is similar to the dimension of the rigid filler[12].

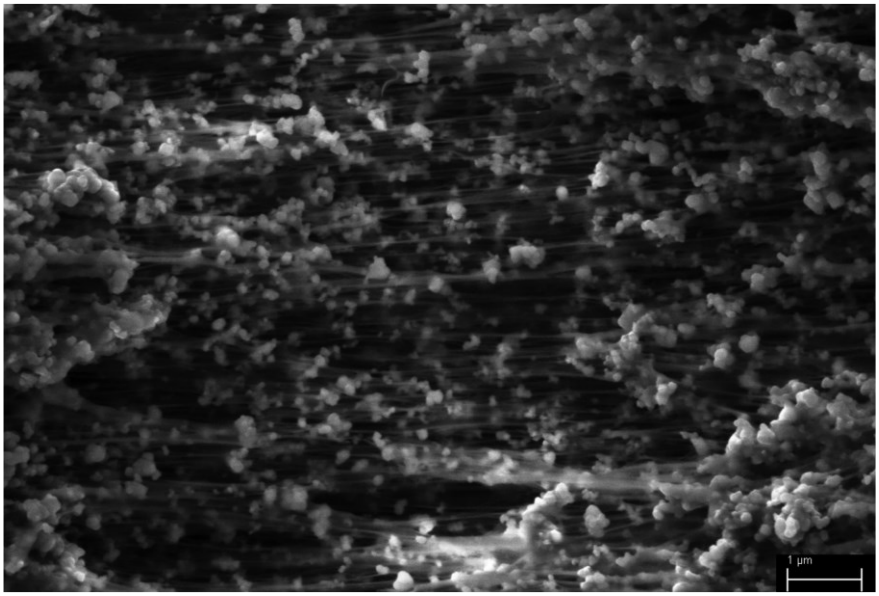


*Figure 6 SEM of NR filled with 150 phr of N772 CB[13].*

### 2.1.5. Models for NR tensile curves

It is well known that most of the mechanical properties of materials can be evaluated thanks to uniaxial elongation experiments. For this reason, it has been always important to find a description of the rubber elasticity through different models, with the aim to describe in the most precise way the "unique" experimental mechanical response of the rubber materials. In rubber mechanics, the molecular description at the base of the models, share three main assumptions: i) the material must be constituted of polymeric chains, and this means that chains are able to change their extension in a dramatic way under stress. ii) the chains must possess high level of mobility, and this means that the mobility of the chain should not be not highly restricted from rigid domains or from too high viscosity iii) the chains are joined in a network structure, and this is connected with the presence of cross-links, coming from vulcanization, which acts as physical bonds and allow the complete recovery of the deformation, or better, they prevent the chains to slide fully in a viscous way.

The chain distance is usually described as the distance end to end r in the x, y, z plane and the initial chain length is $r_0$. The probability of the final position of the end of the chain to be in a particular point of the x,y,z space is often described with a Gaussian distribution function:

$$\omega(r) = \left(\frac{3}{2\pi\, {r_0}^2}\right)^{3/2} \exp\left(-\frac{3r^2}{2\, {r_0}^2}\right) \quad (1)$$

The energy of the chain is referred to the Helmholtz free energy:

$$F(T) = -kTln\big(w(r)\big) = C(T) + \frac{3kT}{2{r_0}^2}r \quad (2)$$

Where C(T) is a constant at the specific temperature T and k the Boltzmann constant. Starting from this point, one of the most common models used to describe the rubber elasticity is the affine model. This model states that microscopic deformations of the cross-links are affine (linear) with the macroscopic deformations observed in the rubber sample, and this means that is possible to obtain the deformation ratios from the lengths of the samples $L_i$:

$$\lambda_i = L_i/L_{i0} \quad (i = x, y, z) \quad (3)$$

From this description is possible to demonstrate that, for uniaxial elongation, the tensile stress will be:

$$\sigma = \frac{n}{V}kT(\lambda - \frac{1}{\lambda^2}) \quad (4)$$

Where n/V is the number of chains n per unit volume V and k is the Boltzmann constant[14].

Another way to write this equation is the one showed by Vieyres[15]:

$$\sigma = \upsilon RT\rho_{NR}\,\psi(\lambda - \frac{1}{\lambda^2}) \quad (5)$$

Where v is the network chain density (mol/cm$^3$), R is the gas constant and $\rho_{NR}$is the density if the rubber. The interesting aspect is the introduction of the parameter $\psi$ which vary, depending on the type of the model used, that can be affine or non-affine. For the affine model $\psi = 1$. The other important model is the phantom model, which states that the chains can be described with a zero cross sectional area, and mostly, the deformations of the cross-links happen with fluctuation in space, those reducing the strain of the chain, which will be lower respect the macroscopic one observed in the sample. In this case the parameter $\psi = f - 2/f$ where f is the functionality of the network.

The issue with these models is that they do not consider real phenomena such strain induced crystallization and the relaxation before the starting of the crystallization. A semi-empirical model which tries to consider this last observation, through the introduction of 2 parameters $C_1$ and $C_2$ , is the Mooney-Rivlin curve[15]:

$$\sigma = 2(C_1 + \frac{C_2}{\lambda})(\lambda^2 - \frac{1}{\lambda}) \quad (6)$$

## 2.2. Strain Induced Crystallization (SIC) and Elastocaloric effect (eC)

### 2.2.1. Crystallization in natural rubbers

The advantage of natural rubber, with respect to many other elastomers, is its ability to crystallize under high deformations (> 200%), and this phenomenon is called strain induced crystallization (Figure 7). During the elongation, the chains tend to orient along the stretching axis, increasing their extension and favouring the possibility of forming oriented crystalline structures[16]. The other route of crystallization is the Temperature Induced Crystallization (TIC), governed by nucleation and growth mechanisms, which is characterized by much lower kinetic respect than of SIC, and the best condition for observing it is at -25°C[17].

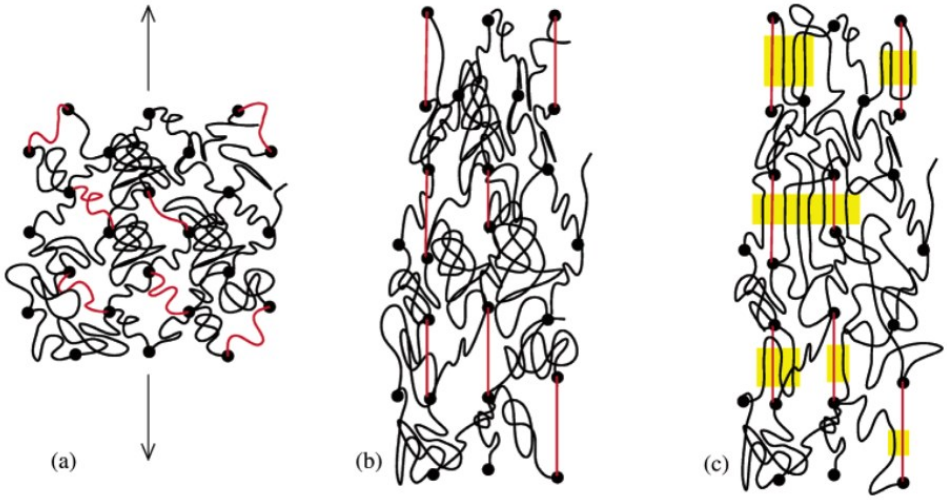


*Figure 7 Schematization of SIC[18]*

The presence of crystalline domains influences the mechanical resistance of the rubber, increasing the tensile modulus in correspondence to high deformations. This self-reinforcement phenomenon is one of the most interesting properties of the rubber, even if until now the mechanisms behind it, in particular the kinetic, are still not completely understood.

Another characteristic of the natural rubber is that it shows stress relaxation at a fixed extension ratio (Figure 8). When the rubber is highly stretched and the crystalline phase is formed, if a constant deformation is maintained, the remaining amorphous chains will exploit the external energy to move in a more disordered state, increasing the entropy, and decreasing the stress[17].

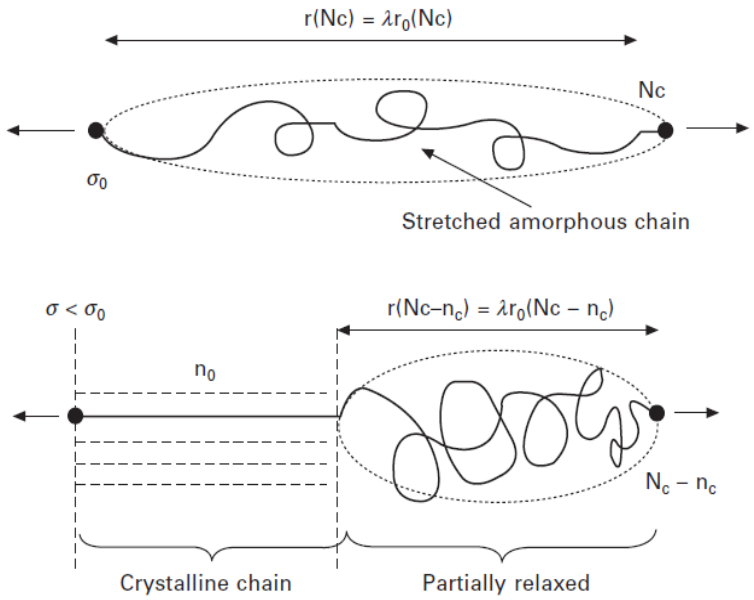


*Figure 8 Stress relaxation in natural rubber[17].*

### 2.2.2. Flory's theory and thermodynamic of SIC

The most important theory related to the SIC, is Flory's theory developed in 1947, which describes the thermodynamic transition from amorphous to crystalline phase of the rubber, similarly to liquid-gas phase transformations. Flory made 3 important assumptions, regarding the behaviour of the chains in crystallization:

The crystallites formed by the chains are perfectly oriented along the stretching direction, and consequently they can't form in the direction perpendicular to the axis.

The chains involved by crystallization can't re-enter in the crystalline phase by folding.

Chain elongations are moderate and can be described with Gaussian statistics.

Firstly, is possible to neglect the volume variation due to crystallization and define the stretching ratio as $\lambda = \frac{L}{Lo} = 1 + \varepsilon$ for a uniaxial tensile test, related to the engineering stress σ. The thermodynamic potential, per unit volume, associated with the elongation of the polymer will be, as proposed by Miyamoto et al:

$$\Omega = U - TS - \lambda\sigma \tag{7}$$

The variation of the potential $d\Omega = -dTS - \lambda d\sigma$ is dependent on two intensive properties σ and T, which define the equilibrium during the phase transition, from amorphous to crystalline phase. The thermodynamic potential $\Omega_N = \Omega(\lambda, \sigma, T)$ is function also of λ, which will be the parameter that distinguishes the 2 phases, correspondent to the elongation of the crystalline phase $\lambda_c$ and the amorphous phase $\lambda_a$. $\Omega_N$ depend also on the average number of statistical segments N, which are related to the cross-link density of the polymer $\upsilon = (1/Na^3)$, where $a^3$ is the volume for statistical segment. Considering a single chain and hypothetically a full crystalline phase, the elongation in the crystalline phase can be written as $\lambda_c = (3N)^{\frac{1}{2}}$.

The potential $\Omega_N = \Omega(\lambda, \sigma, T)$, will have 2 minima for a particular set of T and σ, which will correspond to the potential of the crystalline phase $\Omega_c$and amorphous $\Omega_a$. The equilibrium of the two phases will be reached when $\Omega_c = \Omega_a$ , for which will correspond a melting temperature $T_m(\sigma)$ or equivalently a particular $\sigma_{eq}(T)$. In correspondence of these 2 minima points in the (σ; T) phase diagram we will obtain the two extended ratios $\lambda_c = f(\sigma)$ and $\lambda_a = f(\sigma)$ which will be the two constitutive equations.

Using this model is possible to describe the system with $\sigma(\lambda)$ equilibrium isotherm (Figure 9), in analogy with a Clausius Clapeyron diagram for the liquid-gas systems. Starting with 100% of amorphous phase, the stress is increased until the point C, related to the phase transformation and a correspondent deformation $\lambda_{melt}$ . The amorphous phase is overstretched until point C', following the equation $\lambda_a = f(\sigma)$ ; then the amorphous phase relaxes from C' to C'', with a deformation $\lambda = \lambda_{melt} + \Delta\lambda$ and the related decrease in stress $\Delta\sigma$.

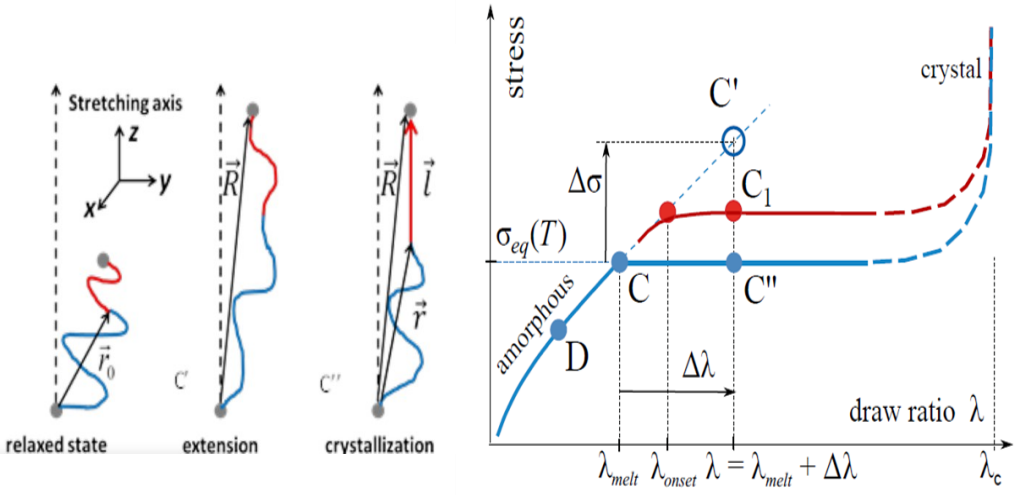


*Figure 9 On the left: Representation on the 3 main stages leading to SIC. On the right: stress-strain curves related to the thermodynamic description by Flory.*

This ideal representation is limited by the kinetics of the crystallization, to which correspond a different behaviour, described better with the red curve in Figure 9. It shows that the onset of the phase transformation happens at higher deformation $\lambda_{onset} > \lambda_{melt}$ , and the related plateau is observed for higher stresses. In correspondence of the plateau is possible to estimate the level of crystallinity χ at a particular stretching ratio λ, using the lever rule:

$$\chi = \frac{\lambda - \lambda_a}{\lambda_a - \lambda_c} \tag{8}$$

In this way, it is demonstrated that the change in crystallinity is dependent on the changes in deformation. In the experimental curves, the plateau related to the relaxation is not highly pronounced and sometimes is even difficult to be observed, as the crystalline phase quickly activate the self-reinforcement mechanism, increasing the rigidity, while the amorphous phase does not have enough time to relax enough due to the strain rate[19].

### 2.2.3. Effect of fillers in SIC

One of the most important fields of interest for improving the mechanical resistance of the natural rubber, is the utilization of reinforcing fillers, such as Graphene Oxide, Carbon black, Silica, or waste rubber waste particles.

Different experiments show that fillers can promote the nucleation of crystals during the elongation of the rubber. As fillers are much more rigid than the rubber matrix, when the material is stretched, the matrix will deform more locally in the region near the fillers to compensate for their null deformation, enhancing the phenomenon of SIC[20]. However, the exploitation of reinforcing fillers and their ability to increase the rigidity during elongation is not always connected to an increase in the toughness of the rubber; and the real dependence between the percentage of fillers and the ability of the material to crystallize during elongation is still controversial. In fact, experimental works show that an increase in toughness with the increase of fillers content happens only up to limited concentrations. For example, the volume of crystallites formed after elongation cannot be such high when using higher fillers content, as the filler restrict the domain for the potential crystallizable volume[16].

### 2.2.4. X-ray diffraction for studying crystalline structures.

For the study of the crystalline phase of the rubber, a fundamental tool is the analysis of the x-ray diffraction patterns. X-rays are electromagnetic waves with wavelengths generally in the range of 0.1-

10 A°. It is well known that the wavelengths of the x-ray beams are similar to the inter-atomic distances between the crystalline planes of the materials, which can be then differentiated thanks to the Miller indices (h,k,l). In this way, when the beam encounters the material, the crystalline phase deviates the path of the ray, with scattering mechanism, with an angle of 2ϑ, which depend on the specific Miller plane. Screens and detectors can then collect the intensity of the scattered beam to produce the diffraction patterns. The equation that relates the wavelength of the x-ray λ and the angle of diffraction ϑ to the interatomic distance d is the Bragg Law[21]:

$$2d_{(h,k,l)}sin\vartheta = n\lambda \tag{9}$$

For the natural rubber, experimental diffraction patterns show the formation of crystals in correspondence of the following planes: (002), (200), (210), (120)[16] as shown in Figure 10:

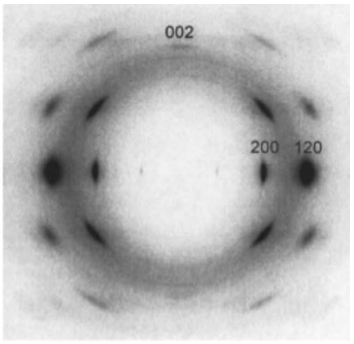


*Figure 10 Example of diffraction pattern for natural rubber[22].*

This tool is especially important for studying the evolution of the crystalline phase during stretching and this can operatively be done through in situ Wide Angle X-ray Scattering in transmission experiments (WAXS). For instance, is possible to evaluate the stretching ratio related to the onset of crystallization and compare it with different operative parameters, such as: strain rate, composition, operative temperature, cycles of loading[16].

One of the obstacles, during the measurements, is the presence of the contribution related to the diffusion of air, or filler particles, such as carbon black, therefore, is important to normalize considering these contributions. For being able to separate them effectively the incident ray must be focused as much as possible, to obtain more pronounced peaks of intensity. An optimal solution is the exploitation of the synchrotron radiation source, which possesses a much higher focusing capability with respect to the lab x-ray technologies[23].

### 2.2.5. Elastocaloric effect of NR

A phenomenon that is strictly connected with strain induced crystallization is the elastocaloric (eC) effect. When the NR is stretched with a tensile force the alignment of the chains and the formation of the crystalline phase is a related to a decrease of the entropy of deformation. This decrease causes a release of heat which will increase the temperature of the rubber during stretching. When the material is unloaded there will be an opposite effect, as the chains will return to a deformed state increasing their entropy and consequently decreasing the T of the material which will cool until returning to its initial length (Figure 11).

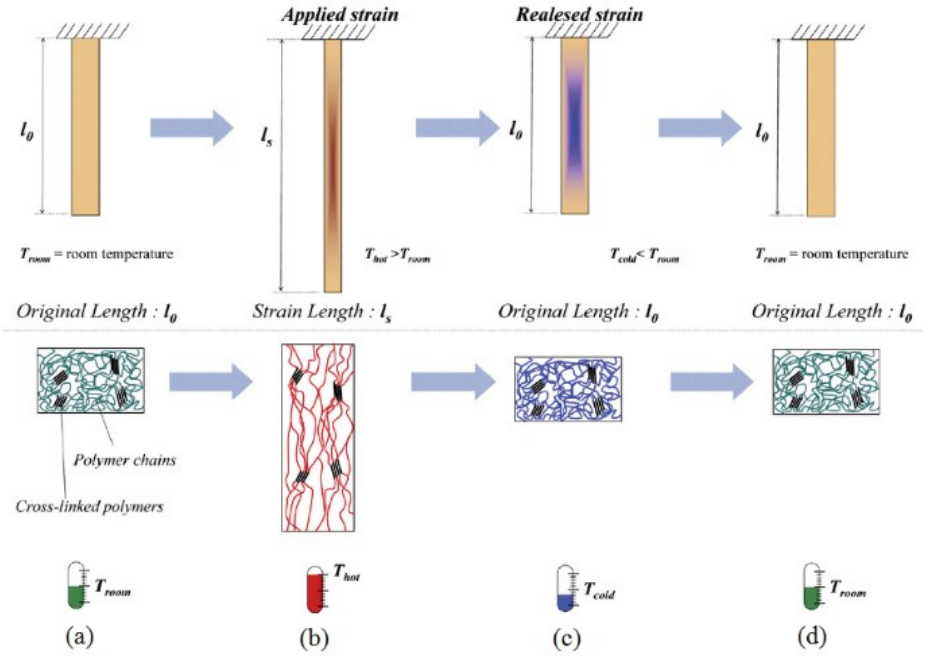


*Figure 11 Elastocaloric effect during loading/unloading of NR[24].*

The strain induced entropy variation after a displacement Δl is expressed as:

$$\Delta S(T, \Delta l) = -\int_{l_0}^{l_1} (\partial F/\partial T)_l dl \tag{10}$$

The consequential adiabatic temperature variation is expressed as:

$$\Delta T_{ad}(T, \Delta l) = \int_{l_0}^{l_1} \frac{T}{C} (\partial F/\partial T)_l dl \tag{11}$$

Where C is the heat capacity of the material, T the temperature and F the applied force. In real conditions there will be always heat dissipation due to internal friction and the material will reduce its elasticity by the fatigue loading, decreasing the maximum achievable $\Delta T$[24]. Is possible to minimize these effects performing tests with high strain rates. However, the mechanisms which control the eC are still controversial and subject to investigation.

This ability to change temperature during loading and unloading, make these materials interesting for heating and cooling applications.

## 2.3. Ground Tires Rubber (GTR)

### 2.3.1. Recycling of GTR

One of the main challenges in the polymer industry is the capability of recycling the waste of rubber coming from the tire production. The rubber used for tires is manufactured using the vulcanization process that we have described before. The creation of strong chemical links in the rubber network, as sulphur bridges, leads to a material that is not anymore fusible and soluble, that therefore loses its ability to be shaped and mixed for its reuse.

The absence of a large-scale recycling of tire rubbers leads to the problem of the end-life of the material. The discharge landfills are not sustainable from both economical, for the cost of transportation, and environmental point of view, for the creation of hazardous gases, accumulation of mosquitos and fire hazard[25]. Another common option is the incineration, which recovers thermal energy from the burning of the rubber, and its advantage consist mainly in a good energy gain respect heat production costs[26]. However, the emissions need to be adequately controlled, limiting the dispersion of hazardous waste and gases[27].

One of the recycling routes that is more followed now from the scientist is the possibility of creating new blends, mixing thermoplastic and ground tire rubber. GTR is used in form of particles, dispersed inside the rubber matrix, acting as a reinforcement. To achieve a good composite, it is important to guarantee a homogeneous dispersion of the GTR in the matrix and especially to guarantee the formation of a strong interface[28]. The only way to increase the solubility of the GTR is through devulcanization processes, eliminating the cross-links coming from the vulcanization process.

### 2.3.2. Devulcanization of GTR

The devulcanization is a process of selective elimination of the sulphur bonds created during the first vulcanization process of the rubber and the biggest challenge is to find methods which are more

selective for the C-S and S-S bonds, respect the C-C bonds of the main chain. Theoretically the selection is achievable, as C-C bonds have higher energy both respect C-S and S-S (Figure 12), but as the main backbone C- C bonds are present in much higher quantity respect the sulphur cross-links and as it is difficult to control accurately the energy transferred to the particles, the degradation of the main chains always happen to some degree, lowering the mechanical properties of the GTR[29].

| Bond Type | Bond Dissociation energy (kJ/mol) |
|---|---|
| C-C | 370 |
| C-S | 310 |
| S-S | 270 |

*Figure 12 Energy of the bonds involved during devulcanization process.*

Many different approaches have been experimented and are used now for the devulcanization, exploiting chemical, thermomechanical and thermal processes.

One of the most used chemical processes is dynamic desulfurization, where the rubber reacts in a tank at high pressure and high T in an aqueous solution with the presence of specific auxiliary agents. This method uses high amounts of water and energy and produces heavy pollution. For these reasons it cannot be considered good for a long-term view, and it will need to be replaced with more sustainable solutions.

Another common industrial method is the reactive extrusion, which is much more environmentally friendly with respect to the dynamic desulfurization. This method, which consists usually of a twin-screw extruder, exploits the high shear forces and the high heat, generated by the screws and the barrel, to provide a good plasticization and a homogeneous distribution of the material. The limitations of this method are connected mainly with the equipment: its high cost, the fixed length of the screw which cannot be enough for achieving the desired degree of devulcanization, and the durability of the apparatus which can be corroded over time[30].

The method, which is now gaining more interest especially in laboratory scale, is the microwave devulcanization. The utilization of common kitchen's microwaves for heating the GTR brings many advantages. Firstly, the microwave radiation, differently from the most common heat sources which exploit the mechanisms of conduction and convection, transfer energy with electromagnetic radiation, which is converted into heat inside the material through atomic interactions, allowing a more homogeneous and volumetric heating of the powder[31]. Another advantage is the process itself: the microwave oven is cheaper than many other equipment and the energy output is precise and easy to manage, as the user can most of the time control the 2 parameters of power and time. It may also

become interesting from an industrial point of view as a good amount of material can be treated in one time (batch-continuous), and the process is environmentally friendly, as it is energy efficient and solvent free. However, when reaching high temperature, another phenomenon to take into-account is the possibility of having re-vulcanization (secondary cross-linking), due to the formation of sulphur's free radicals (Figure). An issue of GTR particles is also their compositional complexity, as they are constituted of different fillers, additives, plasticizers, which can be insoluble and this can lead to a decrease in the efficiency of reinforcement after devulcanization[32].

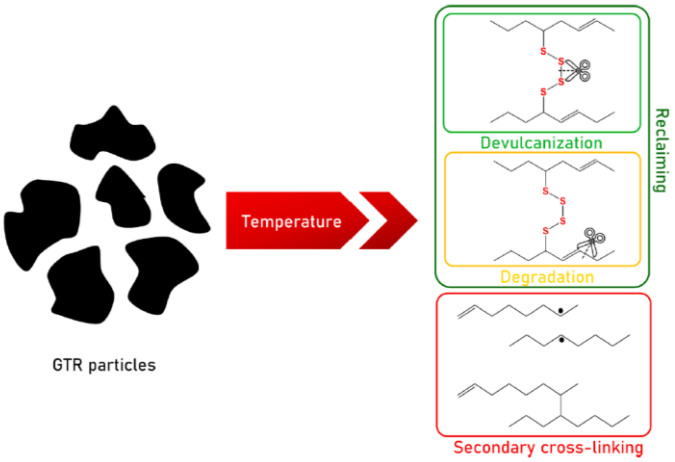


*Figure 13 GTR reactions induced by heating.*

The correct setting of power and time is very sensible to the specific application, and particularly to the type of GTR particles involved and the amount used in every heating session. In literature the most common values of power are between 700-900 W, maintained with times between 1 min and 5 min.

## 2.4. Thermally Conductive Fillers for Natural Rubber

### 2.4.1. Improvement of NR thermal conductivity

Natural rubber is considered a thermal insulator as it present low values of thermal conductivity at different temperatures, usually around 0.1 and 0.3 W/mK. Thermal conductivity k is a property that measure the ability to transfer heat between 2 different points of the material which presents a temperature difference of ΔT. If we exclude the heat transferred by convection and irradiation, the thermal conductivity can be expressed in function of heat exchanged in the material q and the thickness of the material t, in stationary conditions, following the Fourier's law:

$$q = k\frac{\Delta T}{t} \tag{12}$$

The interest in increasing thermal conductivity of the rubber comes from the necessity in different applications to improve the heat dissipation. For example, in tyres, heat management is strongly connected with service life as tyres undergo dynamic loading, and the internal friction of the different components (fillers, NR, SBR) can cause a high amount of heat, with a consequently increase in temperature, which can negatively affect the performance of the component, especially the thermal fatigue.

In order to find solution for improving the conductivity, is important to understand the mechanism involved in heat conduction in polymers. Both in amorphous and semi-crystalline polymers, heat conduction take place mainly thanks to phonons, or better thanks to the propagation of the vibrations between atoms induced by thermal excitation. In the crystalline phase the thermal diffusion is higher respect to the amorphous phase, thanks to the high order of the chains and atoms, which are able to oscillate near their equilibrium position. In the amorphous phase the disordered distribution of the chains and their random orientation hinder the thermal diffusion causing phonon scattering.

One of the solutions for improving the thermal conductivity is the addition of conductive fillers to the polimeric matrix. The idea behind this solution, is to build a filler's conductive network inside the material with the function of creating a preferential path for the phononic propagation. However, even if the percolation threshold seemed to be achievable, there is still no possibility to predict accurately the effect of the conductive fillers in the heat transport. This is mainly due to the high number of parameters which can affect this phenomenon, which are summarized in Figure 14.For example if we consider a matrix with an high amount of conductive fillers, there will be an increase in the thermal resistance of the polymer, due to the high number of polymer/filler interfaces which will act as heat barriers. However , if an higher amount of fillers is present, is much probable to form interconnected clusters and achieve the percolation threshold , increasing the conductivity.

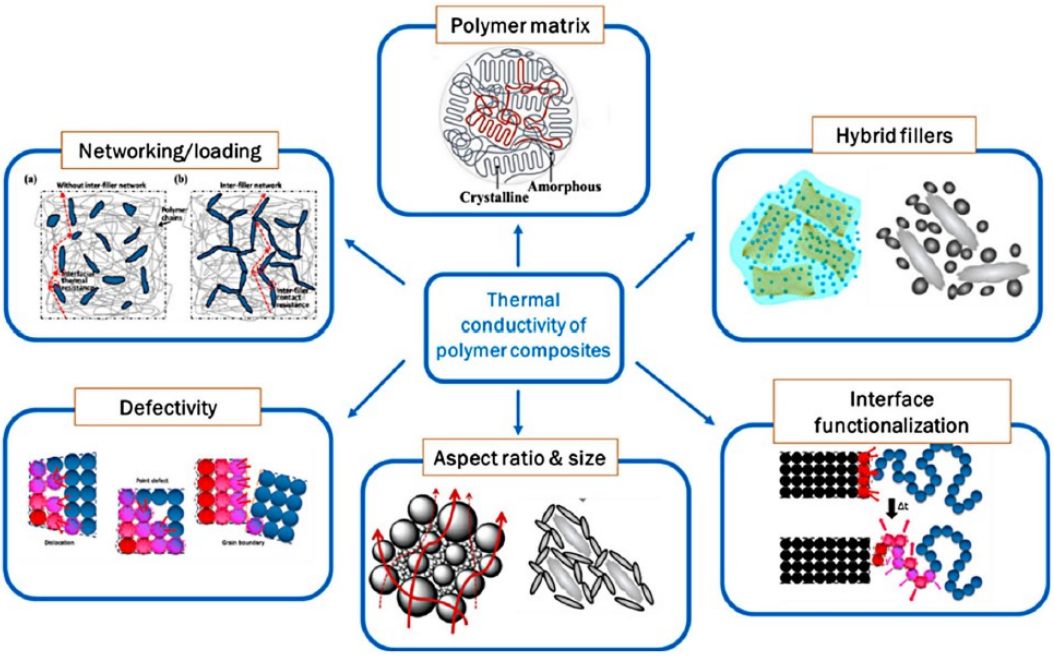


*Figure 14 Parameters influencing the thermal conductivity of NR composites.*

The building of the network will be strongly influenced also by the morphological aspects of the filler's particles and moreover by their spatial distribution, which relates to the ability of achieving a good dispersion during the synthesis of the composite[33]. One of the most investigated solutions for improving the dispersion of the fillers is the synthesis of hybrid fillers, where larger fillers particles are functionalized with smaller fillers particles, which function is to increase the surface activity and reduce agglomeration phenomena and non-uniform dispersion.

### 2.4.2. Carbon based conductive fillers

One of the most important fillers in rubber industry is Carbon Black, which 92% of the production is used in rubber industry, and the most important application is tyre manufacturing. CB started to being used more than 50 years ago, with the purpose of reinforce rubber's mechanical properties. It is well known that CB can improve the tensile strength, modulus, and abrasive resistance. However, CB seems to be a good filler also from the point of view of thermal conductivity, as some articles demonstrated an increase in thermal conductivity even up to 0,42 W/m K with 26,2% of CB. Song et al.[34], investigated the influence of different type of CB in thermal conductivity of NR/CB composites, addressing the mechanism of conductive networks to the particle size and distribution in the rubber matrix. Thanks to TEM images is possible to observe the formation of different aggregates of CB particles that, if present

in enough amount, can form interconnected three-dimensional networks, as showed in Figure 15.

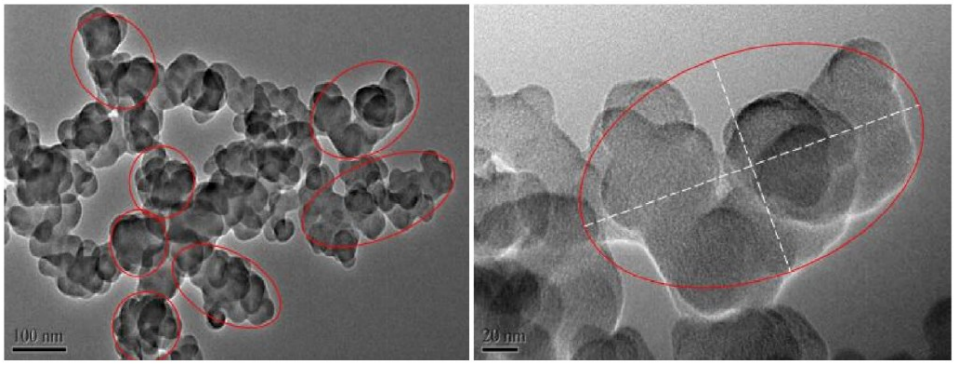


*Figure 15 Examples of CB interconnected aggregates (TEM[34]).*

The formation of aggregates strongly depends on the morphology of the particles, and particularly the surface interactions. For instance, a deep understanding of this aspect will be fundamental for the possible utilization of recycled carbon black (RCB), which can be a further step for the improvement of the circular economy of CB particles. RCB particles seem to show lower surface activity respect the commercial ones, due to the presence of ash in the reactive sites which reduces the active surface area and consequently leads to a poor dispersion in the rubber matrix. Therefore, the research should be focused on the reduction of the ash content and improvement of the surface properties of RCB[35].

Another type of carbon-based conductive fillers are carbon nanotubes. These one-dimensional fillers are interesting for their high mechanical and thermal properties and for this reason they are usually adopted to reinforce natural rubber. Their potential use as thermally conductive fillers lie on the possibility of increasing the conductivity with a very low fraction compared to CB, and consequently decreasing the percolation threshold. For this application carbon nanotubes are used in a multi wallet configuration (MWCNT), and the higher thermal conductivity reached for NR/CNTs compounds is of 0,506 W/mK with only 1,4 wt% of CNTs. The drawbacks of these fillers are mainly their high specific cost and their poor dispersion in the rubber matrices. The low dispersion of the nanotubes increases the probability of forming large agglomerates in the matrix, due to the high Van der Waals forces between the CNTs, leading to higher percolation thresholds. To achieve a better dispersion and increase the chemical reactivity, many researchers tried to oxydize CNTs with different chemical techniques, such as photo-oxydation and oxygen-plasma. Another possibility is to create an hybrid filler , with CNT's functionalized with CB particles as done by Song et al(Figure 16).[36]

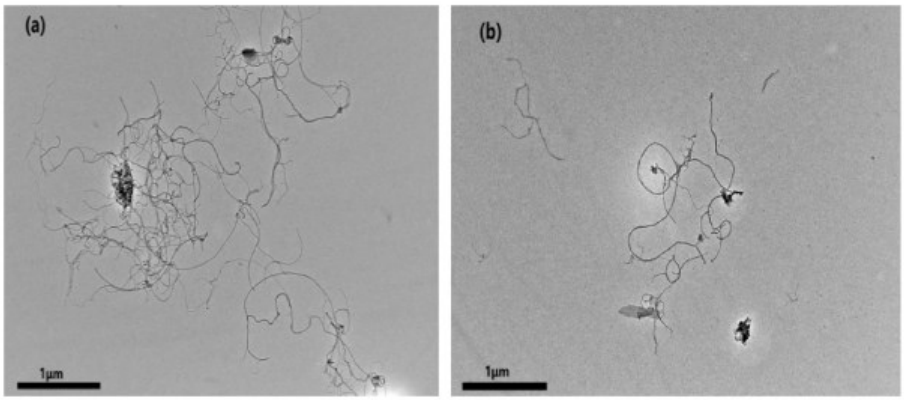


*Figure 16 a) Pristine CNTs b)CNTs functionalized with CB[36].*

# 3. MATERIALS PREPARATION

## 3.1. Natural Rubber (NR)

The natural rubber used for the matrix of the blends is an SMR (Standard Malaysian Rubber) CV60, supplied by the company, Akrochem (Akron, Ohio, USA). The material starting block was of 25 kg and is stored in laboratory at -18°C (Figure 17).

*Figure 17 SMR Natural Rubber.*

## 3.2. Ground Tire Rubber (GTR)

### 3.2.1. Raw materials

The Ground Tire Rubber particles (Figure 18) were obtained through cryo-grinding of tyres and were provided by the company J. Allcock & Sons Ltd. (Manchester, UK).

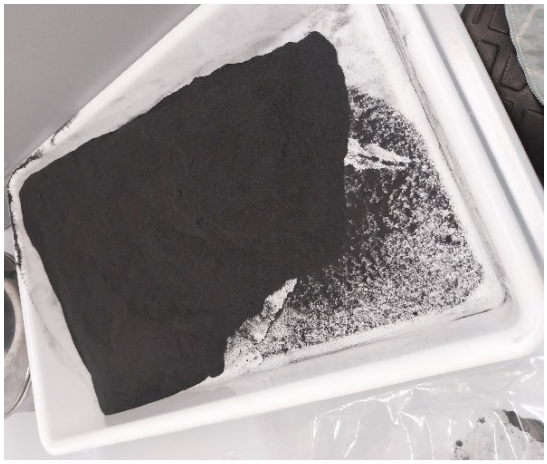

*Figure 18 Ground Tire Rubber particles.*

### 3.2.2. Sieving

The GTR powder was sieved using a vibratory sieve shaker (Analysette 3, Fritsch, Idar-Oberstein, Germany), imposing 4 minutes of vibration with an amplitude of vibration of 1,5 mm for every batch performed. 2 sifters were used, one of 63 µm (ANALYSENSIEB) and another of 100 µm (Fisher Scientific), showed in Figure 19. In this way we obtained 2 different ranges of particle sizes:

1) 63 µm < d < 100 µm, used for the devulcanization experiments for the preparation of NR/GTRd composites.
2) d < 63 µm, stored for future application.


*Figure 19 Sifters for 63 µm and 100 µm sieving.*

### 3.2.3. Microwave devulcanization

The apparatus used for the devulcanization is a domestic microwave, model Electrolux 27E with a maximum output power of 800 W. A hole in the upper wall of the microwave was created in order to place a stirrer, made of Teflon, needed for the homogenous mixing of the powder during heating operation (Figure 20). The stirrer is set with a constant rotation speed of 100 rpm.

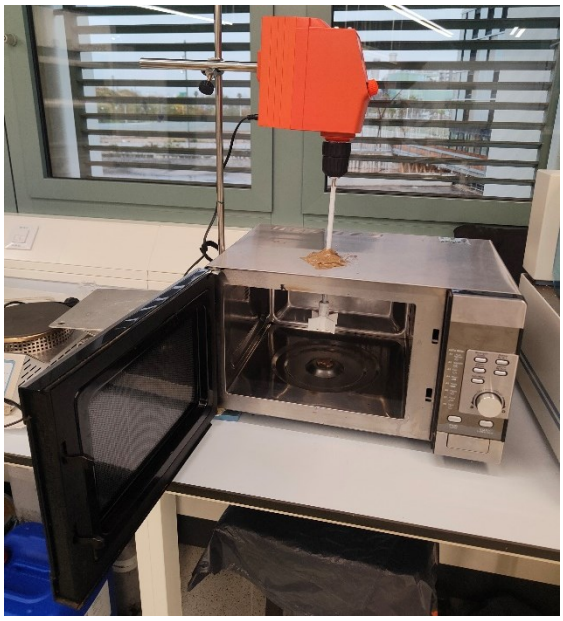

*Figure 20 Microwave apparatus for devulcanization.*

For every batch of devulcanization, 10 g of GTR powder was put inside a becker, and the stirrer was placed in the center of the becker. The energy output of the microwave is:

$$E = P\ t \tag{15}$$

Where P(W) is the power of the microwave and t(s) is the time set for every power. Is important to notice that the energy output of the microwave will be higher than the energy absorbed by the powder, as part of the heat will be absorbed by the glass of the becker. Different sets of time and power were tested in these experiments:

- 800 W with different t=1,2,3,5 minutes
- 640 W with different t= 1,2,3,5,10 minutes
- 400 W with different t=1,2,3,5,10 minutes
- 80 W with different t=1,2,3,5,10 minutes

The nomenclature of the devulcanized GTR particles treated at different conditions will be in the form of GTRDx_y, where x refers to the different powers (80,400,640,800) and y refers to the different devulcanization times (1,2,3,5,10). The names are summarized in the following table:

*Table 1 Nomenclature of devulcanized GTR*

| Material | Power(W) | Time(min) |
|---|---|---|
| **GTRD_0** | **0** | 0 |
| **GTRD80_1** | **80** | 1 |
| **GTRD80_2** | **80** | 2 |
| **GTRD80_3** | **80** | 3 |
| **GTRD80_5** | **80** | 5 |
| **GTRD80_10** | **80** | 10 |
| **GTRD400_1** | **400** | 1 |
| **GTRD400_2** | **400** | 2 |
| **GTRD400_3** | **400** | 3 |
| **GTRD400_5** | **400** | 5 |
| **GTRD400_10** | **400** | 10 |
| **GTRD640_1** | **640** | 1 |
| **GTRD640_2** | **640** | 2 |
| **GTRD640_3** | **640** | 3 |
| **GTRD640_5** | **640** | 5 |
| **GTRD640_10** | **640** | 10 |
| **GTRD800_1** | **800** | 1 |
| **GTRD800_2** | **800** | 2 |
| **GTRD800_3** | **800** | 3 |
| **GTRD800_5** | **800** | 5 |

The values of the nominal power were limited by the possibles choices of the microwave. After the devulcanization, the temperature of the powder was immediately measured thanks to 2 digital thermometers (Figure 21), one with contact (HANNA) and one with laser mechanisms (Raytek).


*Figure 21 On the left, contact digital thermometer (HANNA). On the right, laser digital thermometer (Raytek).*

## 3.3. Vulcanizing agents and Additives

To improve the mechanical properties of the blends and ensure an optimal vulcanization process different additives were used during the mixing of the blend (Figure 22).

Sulphur powder with S -325 mesh, 99.5 % of purity was used as vulcanizing agent. Other additives to improve vulcanization process were Stearic Acid with 97% of purity, used as a vulcanizing activator and *N*-Cyclohexyl-2-benzothiazolylsulfenamide 95-33-0, known also as CBS, with 98% purity was used as vulcanizing accelerator.

N1-(4-Methylpentan-2-yl)-N4-phenylbenzene-1,4-diamine, known as 6 PPD, was used as stabilizing agent and antioxidant, and Zn0 were used to protect the Rubber from UV light degradation.

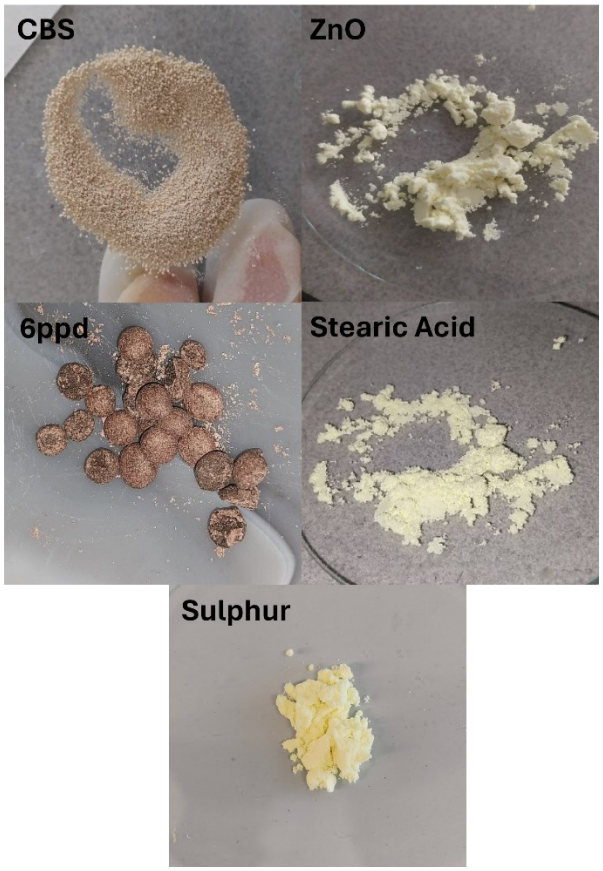


*Figure 22 Vulcanizing agents and additives.*

## 3.4. Internal mixing

The preparation of the NR/GTRD composites was performed using an internal mixer (Brabender) with a volume of the chamber of 55 $cm^3$. The 2 screws of the mixer worked at a rotation speed of 40 rpm and the operative temperature was maintained at 80°C for all the process.

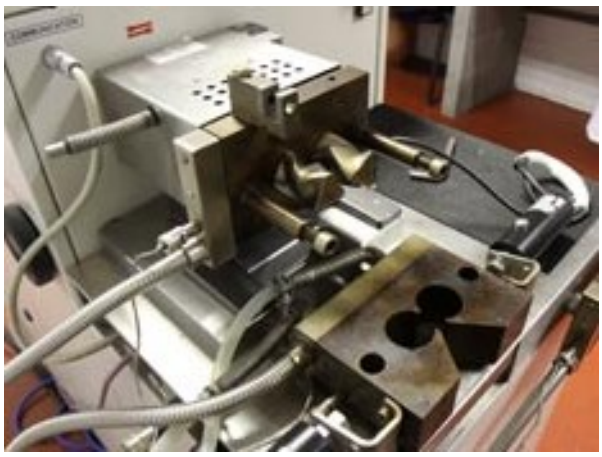

*Figure 23 Internal mixer for blending (BRABENDER).*

The NR, reduced firstly in small pieces, was masticated for 5 minutes; then Stearic Acid, ZnO and 6ppd were inserted to the mixer. After 8 minutes CBS and Sulphur powder were added, and after 10 minutes also the GTRD powder devulcanized at 800W. The blend was keeping mixed until 15 minutes and the final material is represented in Figure 18.

*Figure 24 NR/GTRD blend.*

The composition of the 5 NR/GTRD800 blends is summarized in the following table:

*Table 2 Composition of NR/GTRD800 blends*

| | NR | GTRD800 | Stearic Acid | ZnO | CBS | 6ppd | Sulphur |
|---|---|---|---|---|---|---|---|
| **wt%** | 100 | 20 | 2 | 1,5 | 2,38 | 3 | 1,65 |
| **Mass (g)** | 32 | 8 | 0,64 | 0,48 | 0,76 | 0,96 | 0,53 |

## 3.5. Compression Molding and Hot pressing

After the blending, the material is compressed and vulcanized by hot plate press, model QAP LAP PL-15 s (IQAP Masterbatch SL, Barcelona, Spain). The blend is first cut in small pieces and distributed in a Teflon foil, which protect the material from the direct heat of the hot plates, inside a square aluminium frame of 150 mm wide and 1 mm thick. The 2 hot plates of the machines are heated and maintained at T=170°C with a P=50 bar for 12,5 minutes to perform the vulcanization of the material (Figure 25).

*Figure 25 Hot press for molding and vulcanization.*

## 3.6. Stamping

Once the blend is moulded in the hot press, it is cooled down at room temperature and it is ready to be stamped. The sample for the tensile and cyclic test were stamped by die-cutting with a specimen preparation punching machine (CEAST) (Figure 26).

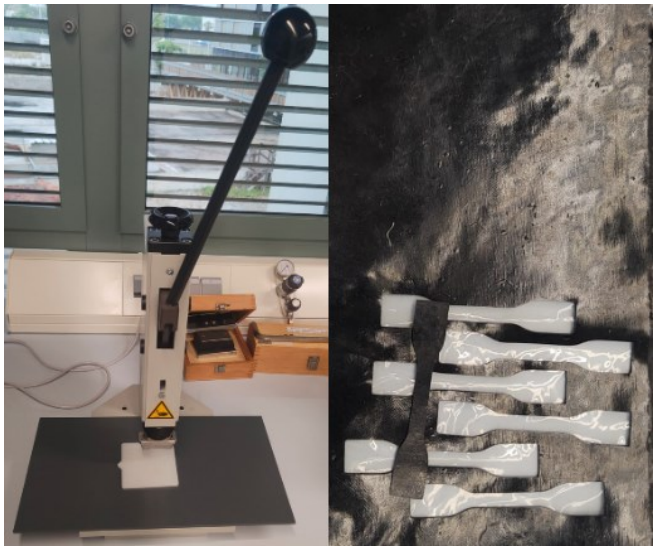

*Figure 26 Stamping machine and NR/GTRD sample.*

# 4. EXPERIMENTS

## 4.1. In situ WAXS and mechanical tests at synchrotron ALBA

We performed in situ WAXS experiments at synchrotron ALBA in Cerdanyola del Vallès (Barcelona), using the beamline BL11 - NCD-SWEET. The layout of the beamline is represented in Figure 27.

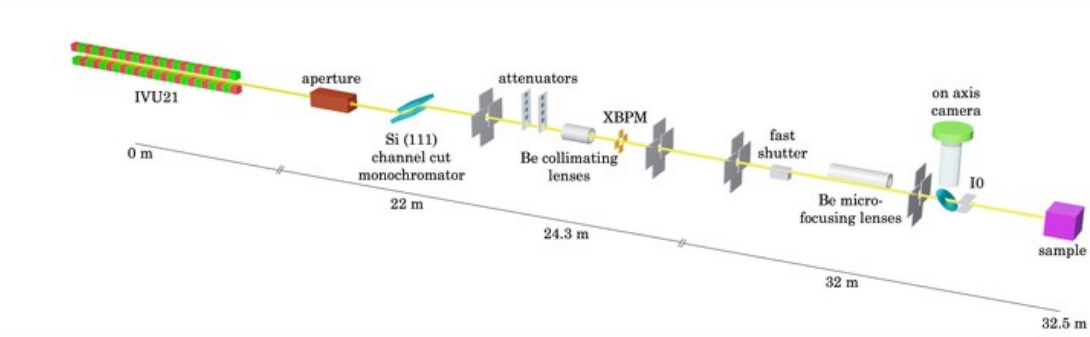


*Figure 27 Schematization of the beamline BL11-NCD-SWEET of ALBA synchrotron.*

The source of the radiation is the in-vacuum undulator IVU21, which delivers a high photon flux, with excellent collimation, photon density and stability over time. The beam first pass through a Si (111) monochromator then it is collimated thanks to Be lenses. Vertical and horizontal slits are used for defining and cleaning the X-ray beam. Before the sample, a fast shutter is used, which can block the radiation if the beam is not needed, to reduce as much as possible, the exposure of the sample.

The beam hitting the sample has a wavelength of 0,957 $A°$ and the time of exposure of the sample is of 1 s. The latency time, needed for the acquisition of the diffraction image vary depending on the different tests: for stretching and de-stretching of the sample at fixed temperature the latency is of 5,1 s, for heating and cooling of the sample at constant deformation the latency is respectively of 19 and 29 s. A single hybrid-pixel photon counting detector, model LX255-HS (Rayonix), with an active area of 85 x 255 $mm^2$ , composed of 1920 x 5760 pixels with a pixel size of 88,54 x 88, 54 $\mu m^2$ , is positioned perpendicularly to the beam for the acquisition of the images . The distance between the detector and the sample is of 229.860 mm.

The sample positioning system used, is the Stretcher - TST3508 (Figure 28), which is capable of temperature and force control, with a force resolution of 0,01 N and a maximum stretching amplitude of 4,5 cm.

*Figure 28 Stretcher - TST350 for uniaxial tensile tests.*

The limited stretching amplitude permitted us to perform tensile tests only up to 300-350% deformations, which didn't allow us to fully investigate the hyper-elastic behaviour of the polymers but was enough to guarantee the possibility of studying the mechanisms influencing SIC, which we already know starting at around 200% deformation, combining the mechanical responses with the diffraction images.

The experimental stress is evaluated from the force applied by the machine F as:

$$\sigma_{exp} = \frac{F}{A_0} \tag{13}$$

Where $A_0$ is the starting cross-sectional area of the sample:

$$A_0 = w\,t \tag{14}$$

With w = 4 mm the width of the sample, and t the thickness of the sample, measured with the Micrometer (INSIZE)(Figure 29).


*Figure 29 INSIZE Micrometer for thickness measurements.*

We evaluated NR/GTR composites, which were made with the same process used for the preparation of NR/GTRD blends, but in this case the NR is vulcanized using 1,5 phr of DCP (dycumil peroxide) and the ground tire rubber is taken with particle size < 63 μm and it is not devulcanized.

We performed different types of mechanical tests for different compositions:

1) Uniaxial tensile tests, reaching maximum deformation or rupture of the sample, performed at ambient temperature T= 25°C and strain rate V2= 10 mm/min.

These tests were done for the following compositions: NR, NR/GTR10, NR/GTR20, NR/GTR33, NR/GTR40.

2) Uniaxial tensile tests, reaching maximum deformation or rupture of the sample, performed at ambient temperature and with different strain rates, listed below:

**V1** = 60 mm/min **V2** = 10 mm/min **V3** = 1 mm/min

These tests were done for the following compositions: NR, NR/GTR10, NR/GTR20. Unfortunately, the NR samples showed un-expected behaviours, due to technical problems and for this reason, the results concerning the NR at different strain rates will not be discussed.

3) Uniaxial tensile tests, reaching maximum deformation or rupture of the sample, performed with strain rate V2= 10 mm/min at different temperatures, listed below:

**T1=**50°C **T2** = 25°C **T3**= -25 C° **T4**= -40 °C

These tests were done for the following compositions: NR, NR/GTR10, NR/GTR20.

4) Cyclic tests, loading until maximum deformation and unloading the material until reaching a null force, performed at ambient temperature T= 25°C and strain rate V2= 10 mm/min.

These tests were done for the following compositions: NR, NR/GTR10, NR/GTR20, NR/GTR33, NR/GTR40.

5) Loading thermal cycles: these tests were a combination of uniaxial tensile test and variation of temperature at fixed strain. Firstly, the sample was stretched at ambient temperature until achieving the maximum elongation of the Stretcher. Once achieved, the sample was kept at fixed deformation passing to a heating stage, where the temperature was increased up to 120°C with a heating rate of 0,05 °C/s. Then the sample was cooled down to room temperature with a cooling rate of 0,033 °C/s using liquid nitrogen.

The tests were done for the following compositions: NR, NR/GTR10, NR/GTR20, NR/GTR33, NR/GTR40. Unfortunately, only 1 sample of NR survived to the entire cycle, while the other samples broke during

heating. This still allowed us to collect information about the fracture mechanisms at high temperatures and relaxation of the composites.

The analysis of the diffraction patterns and the characterization of the crystalline phase will not be discussed in the present work. Diffraction images will be used only as a tool to confirm qualitatively the mechanical response of the samples.

## 4.2. FTIR spectroscopy

FTIR spectroscopy was performed for the characterization of the devulcanized GTR powder with a Nicolet 6700 FT-IR Spectrometer (ThermoScientific, USA). The samples were compacted in pills with a quantity of few milligrams of GTR powder and KBr, which is highly transparent in this range of wavelengths. The range of wavenumbers collected was between 200 and 4000 $cm^{-1}$. The software of the machine collected the data as transmittance as function of the wavenumber (Figure 30).

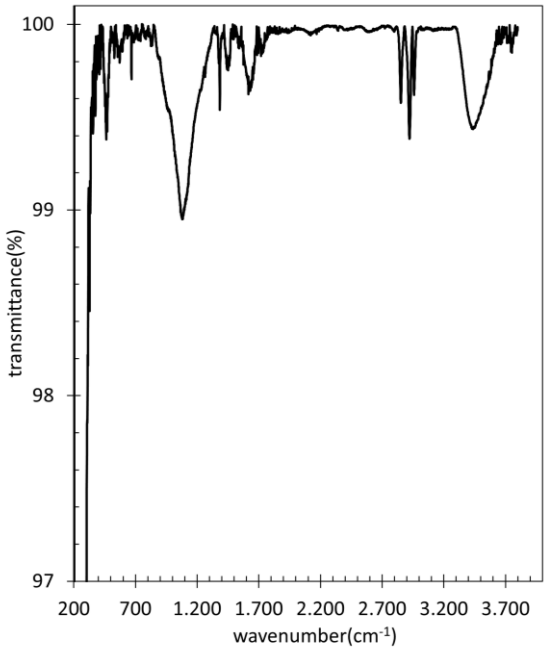


*Figure 30 Example of FTIR spectrum of devulcanized GTR.*

The peaks which need to be analyzed are the one related to the sulphur bonds C-S and S-S, and the bonds related to the main polymeric chain C-H and C-C. The wavenumbers related to S-S and C-S are respectively around 464 and 669 $cm^{-1}$, while the wavenumbers related to C-H and C-C bonds are respectively around 1045 and 2090 $cm^{-1}$.

The intensity of each peak was evaluated subtracting the background values from the maximum values in transmittance. The intensity of the C-S, S-S, C-C bonds were then compared with the ones of C-H bonds in the form of ratios SS/CH, CS/CH, CC/CH.

## 4.3. Swelling

Swelling tests were performed to estimate the cross-link density of the different systems: NR/GTR composites and devulcanized GTR particles. For every composition and materials 3 samples were evaluated, and the final properties will be the average of these 3 measurements. The samples, with a weight of the order of a 150-250 mg, were immersed in cyclohexane solution for 72 h (Figure 31) replacing the solvent every 24 hours, then the swollen mass was measured $m_{wet}$. The samples where than left under fume hood for 72 hours to dry and the dry mass was measured $m_{dry}$. The swelling ratio of the material is evaluated as:

$$Q = \frac{\frac{m_{wet} - m_{dry}}{\rho_{solvent}} + \frac{m_{dry}}{\rho_{NR}}}{\frac{m_{dry}}{\rho_{NR}}} \quad (16)$$

Where $\rho_{solvent}$= 0,778 g/cm$^3$ is the density of the cyclohexane and $\rho_{NR}$= 0,91 g/cm$^3$ is the density of the natural rubber. If the fillers (CB) do not contribute to the swelling of the material, we adopted the Kraus correction for the evaluation of the swelling ratio of the composite $Q_c$ as:

$$Q_c = \frac{Q - \varphi}{1 - \varphi} \quad (17)$$

Where $\varphi$ is the volumetric fraction of the filler in the composite. The volumetric fraction of CB $\varphi_{CB}$ in GTR particles can be estimated by the mass fraction of CB $w_{CB}$ , obtained from the TGA measurements, and NR $w_{NR}$ and the densities $\rho_{CB}$= 1,9 g/cm$^3$ and $\rho_{NR}$= 0,91 g/cm$^3$. The volumes of CB and NR in 1 g of GTR will be $V_x = w_x/\rho_x$ and total volume $V_t = V_{CB} + V_{NR}$. The volume fraction of CB will be $\varphi_{CB} = V_{CB}/V_t$. From this we can evaluate the CB fraction inside the composites NR/$GTR_X$ as:

$$\varphi = \varphi_{CB}\, \varphi_{GTR} \quad (18)$$

Where $\varphi_{GTR}$ is the volume fraction of GTR particles in the composites (10% to 40%). From the swelling ratio, we can consider $v_2 = 1/Q_c$ and then we calculated the cross-link density (mol/cm$^3$) using the Flory-Rehner derived equation:

$$\nu = \frac{\ln(1-\nu_2) + \nu_2 + \chi_1 \nu_2}{V_1(-\nu_2{}^{\frac{1}{3}} + \frac{2}{f}\nu_2)} \quad (19)$$

where $V_1$ = 108 $cm^3$/mol is the specific volume of cyclohexane and $\chi_1$= 0,353 is the Flory-Huggins natural rubber/cyclohexane interaction term, considering also in this case the assumption of the fillers nonparticipating at the swelling. The networks are considered as tetrafunctional and so the value of functionality f =4.

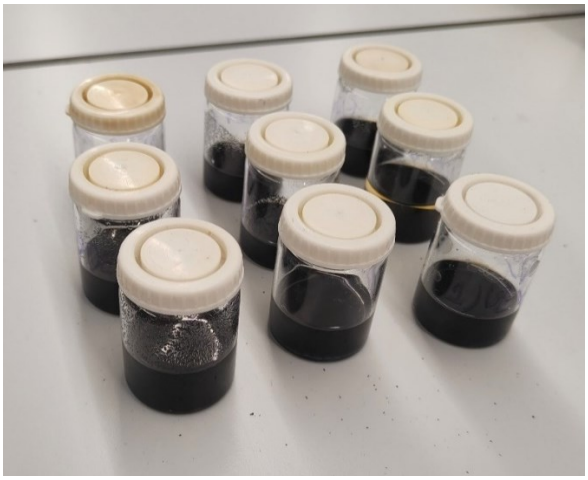

*Figure 31 Samples for swelling test of GTR devulcanized powder.*

For NR/$GTR_X$ samples we also evaluate the soluble fraction s, measuring the dry mass before the swelling experiments $m'_{dry}$ and the dry mass after the experiments $m_{dry}$:

$$s[\%] = \frac{m'_{dry} - m_{dry}}{m'_{dry}} \times 100 \quad (20)$$

## 4.4. Thermogravimetric Analysis (TGA)

Thermogravimetric analysis, using a STARe system (Mettler Toledo, Columbus, OH, USA)(Figure 32), was performed for the devulcanized GTR particles to understand the effect of the devulcanization process on the composition, and particularly to monitor the fraction of carbon black, which is the compound mainly responsible for the mechanical reinforcement of the natural rubber.

*Figure 32 Machine and gas regulation system for TGA.*

Tests were realised following the standard IEC 60811 for the determination of the CB content, using between 5 to 10 mg of powder in an $Al_2O_3$ crucible. The test consists in a heating ramp at 20K/min from 100°C to 950°C performed in 100% N2 environment from 100° to 850 °C and 30%N2 -70% Dry air environment from 850 °C to 950°C(Figure 33). The flux of N2 is of 100 $cm^3$/min while the one of air is of 230 $cm^3$/min.

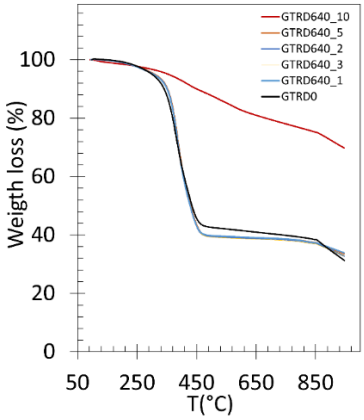


*Figure 33 Example of TGA test performed for GTRD with 640W.*

The weight fraction of CB in the sample is evaluated as the sum of the weight loss between 850 and 950 °C and the weight remained at the end of the test, both in percentage respect the starting mass.

## 4.5. Mechanical tests with Infrared Camera

Mechanical tests with the utilization of a ZwickIII -Expert/Roell tensile testing machine and Infrared Camera were made to study the elastocaloric properties of NR/GTRD800 blends (Figure 34). 3 tensile tests and 1 cyclic test were performed for every sample, both with a strain rate of 3000 mm/min.

Tensile tests were done until rupture of the material, while cyclic tests were performed with a first stretching until ε=500%, maintenance of the deformation for 60 seconds, and then unloading.

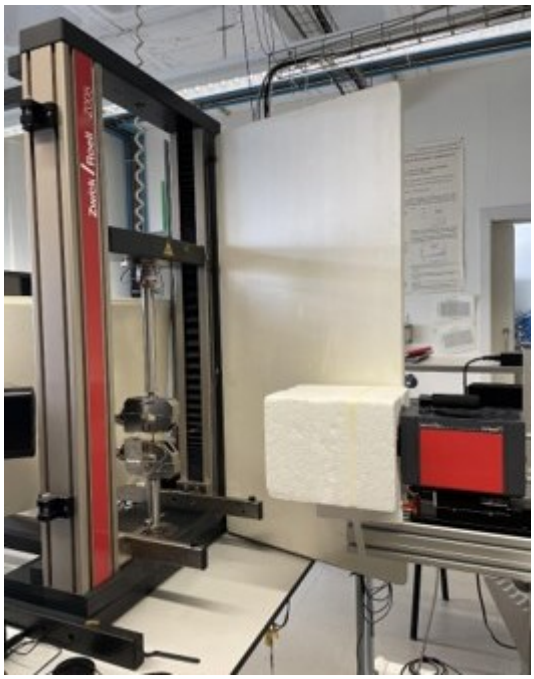

*Figure 34 On the left the tensile testing machine. On the right the IR camera.*

Engineering stress is calculated using equations (13), (14).

The evolution of the temperature along the surface of the different samples was registered by the infrared camera (InfraTech, ImageIRR 8800) with a Mercury-Cadmium-Telluride (MCT) detector, set up at a frequency of 100 Hz and with a temperature resolution at 30 °C higher than 0.035°C.

The distance between the camera and the sample was of 60 cm, to ensure the detection of the temperature with enough precision and of the displacement of the sample. Temperature, Displacement and Force were detected by the camera along 25 points of the sample, homogeneously distributed along the length. The IR camera images were acquired thanks to the IRBIS 3.1 professional software as shown in Figure 35.

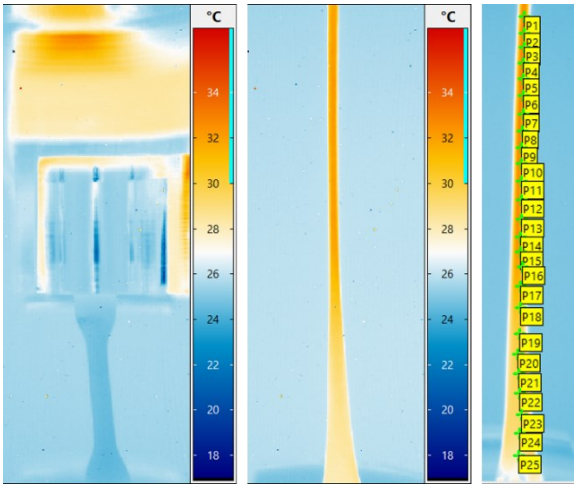


*Figure 35 Evolution of the temperature of the samples with IR camera.*

## 4.6. Field Emission Scanning Electron Microscope (fe-SEM)

For the study of the fracture mechanisms of NR/GTR samples FE-SEM was performed with Neon40 Crossbeam™ workstation (Carl Zeiss) (Figure 36). The electron beam is generated with a Shottky-Fe gun, working at 5 kV with 1.1 nm resolution. The detector is an EDS INCAPentaFETx3 detector with an active area of 30 $mm^2$. The images are processed by a Phenom XL Desktop SEM acquired from PhenomWorld with a resolution below 14 nm and a magnification range of 80-100,000x.

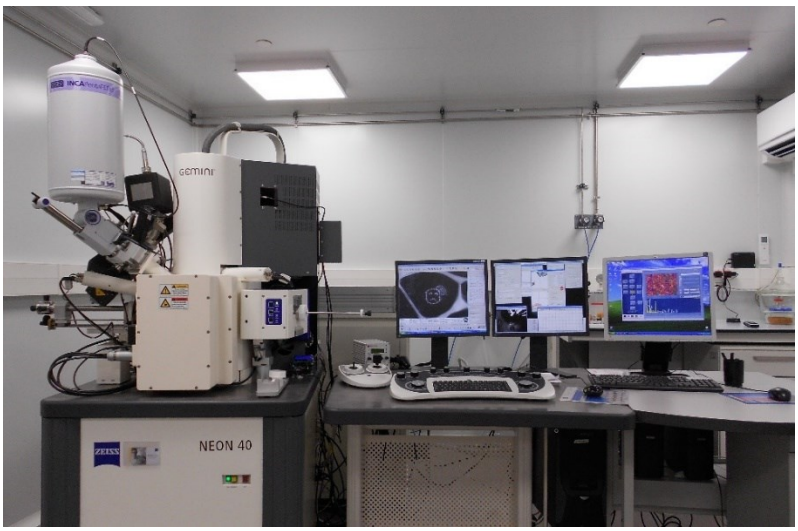


*Figure 36 fe-SEM machine and desktops.*

The 4 samples were prepared cutting in half the samples used in the loading thermal cycle test described in chapter 4.1.. The NR/GTR was firstly attached to a metal sample holder in transversal direction with a carbon adhesive belt. In this way the fracture surface is directed perpendicularly to the electron beam. To increase the conductivity of the samples a silver painting was firstly applied in

the sample surface, then with the utilization of a gold sputter coater EM-ACE600 (LEICA) working in vacuum at a pressure of $10^{-4}$bar with a 30-mA current and a tilt angle of 0°, we applied a 20 nm coating using a carbon thread (Figure 37).

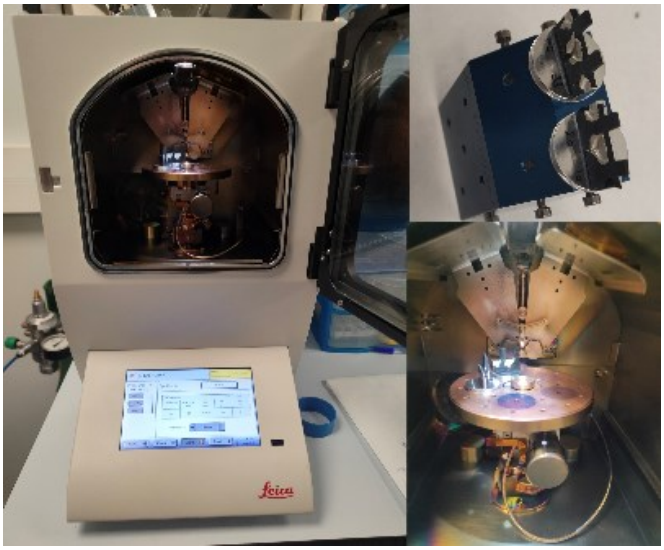

*Figure 37 Coating process with sputtering.*

# 5. RESULTS AND DISCUSSION

## 5.1. NR/GTR composites characterization

### 5.1.1. Swelling of NR/GTR

Swelling experiments performed on NR/GTR samples allowed to estimate the cross-link density using Flory-Rehner thermodynamic description. This description is based on an affine model, and the cross-links are considered with tetrafunctional networks. Also, the Flory-Huggins parameter χ, is assumed to be constant for a particular polymer-solvent couple, even if different experimental works showed a dependence of χ on the volumetric fraction of the polymer[37]. This set of assumptions may cause some uncertainties in the values obtained.

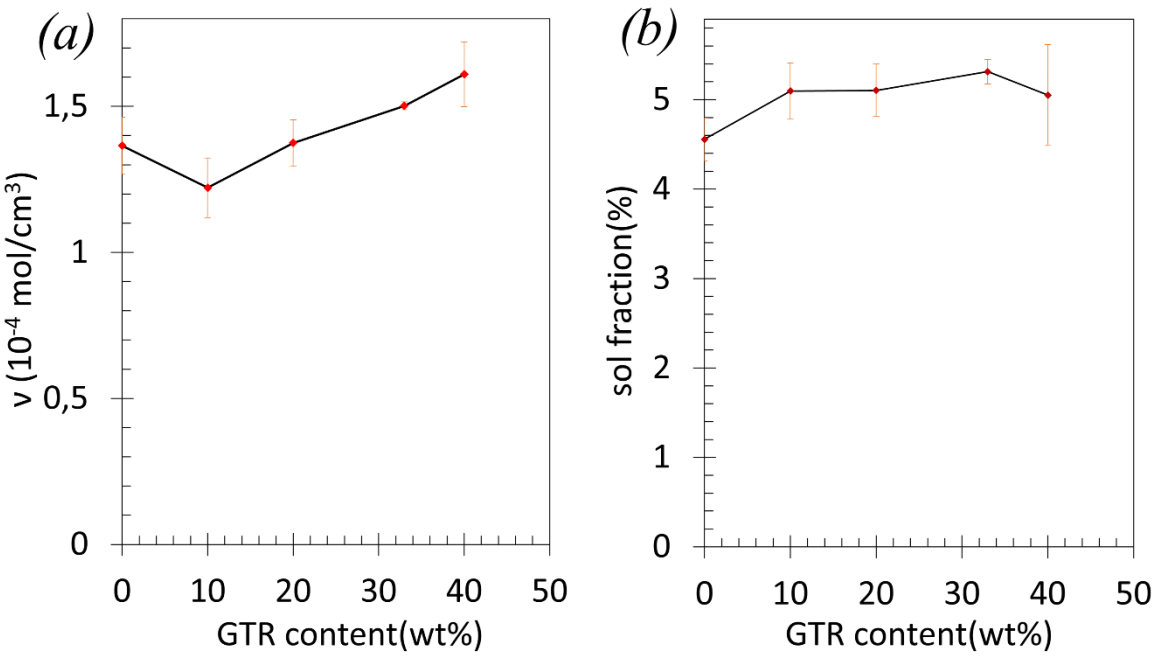


*Figure 38 a) Cross link density of NR/GTRx samples b) Soluble fraction of NR/GTRx samples.*

Experimental data reported in Figure 38 shows that the cross-link density of the polymer tend to rise with a higher content of GTR particles. It is possible that the presence of the filler's act as an obstacle for the penetration of the solution inside the polymer. The lower cross-link density of the NR/GTR10 sample can be related to a poor vulcanization process, as for instance, we observed also lower tensile properties of this material in the previous chapters. It is quite unexpected to observe that the NR/GTR samples have higher soluble fraction respect the NR, as they present higher cross-link density, even if

the difference between them is very little. It is possible that the GTR particles contain some elements that have easier solubility in cyclo-hexane respect the pure NR matrix.

### 5.1.2. Mooney-Rivlin model for tensile tests and strain induced crystallization.

Starting from the stress-strain curves obtained for the different formulations at T=25°C and strain rate of V2= 10 mm/min we will discuss the different behaviour between the experimental stress-strain curves and the ones obtained with Mooney Rivlin model (MR)(Figure 39), to deduce the onset of strain induced crystallization $\lambda_c$. The first important observation is that stretching ratio of the samples containing fillers will be different respect to the one considered for the samples of natural rubber, as filler particles cause perturbation of the local stress of the matrix, those increasing the stiffness of the material. This reinforcement effect can be taken into account considering the "Theory of filler reinforcement" by Guth, who proposed the following correction for the Elastic Modulus in the linear region[38]:

$$E^* = E[1 + 2{,}5\varphi + 14{,}1\varphi^2] \tag{21}$$

Where the increase of the Modulus is dependent on the filler volume concentration φ, calculated as for the swelling experiments with the equation (9). Applying the same observations for the elastic deformation of the material we can define a local strain, starting from the macroscopic deformation ε, as:

$$\varepsilon_{loc} = \varepsilon A \tag{22}$$

Where A, is the strain amplificator factor[16]:

$$A = 1 + 2{,}5\varphi + 14.1\varphi^2 \tag{23}$$

Therefore, the local strain ratio will be:

$$\lambda_{loc} = 1 + \varepsilon_{loc} \tag{24}$$

At the end the MR curve for the NR/$GTR_X$ will be:

$$\sigma_{MR} = 2(C_1 + \frac{C_2}{\lambda})(\lambda_{loc}{}^2 - \frac{1}{\lambda_{loc}}) \tag{25}$$

As the hypothesis of the MR theory is based on Hooke's Law description of the strain energy, we need to observe that the model can describe the mechanical behaviour of the rubber only up to limited deformations (200%). The evaluation of the constants $C_1$ (MPa) and $C_2$ (MPa) for the building of the

MR curves were deduced with the Least Square Method, minimizing the difference of the stresses between the experimental and MR curves up to 150% deformation.

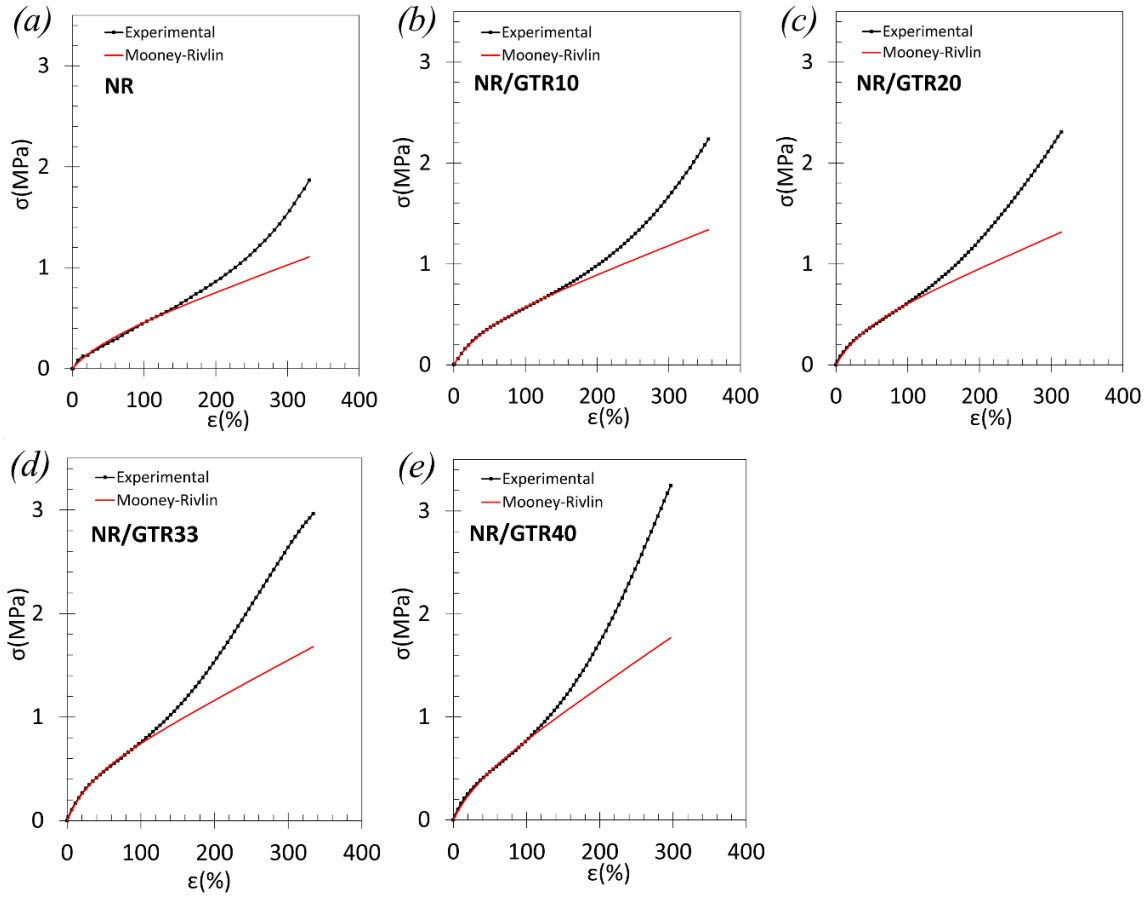


*Figure 39 Experimental and Mooney-Rivlin stress-strain curves for different NR/GTRx composites.*

In literature, the constant $C_1$ is associated with the Young's Modulus in the linear region, in particular for very small deformations (λ≈1), with a relationship[15]:

$$E \approx 2(C_1 + C_2) \tag{26}$$

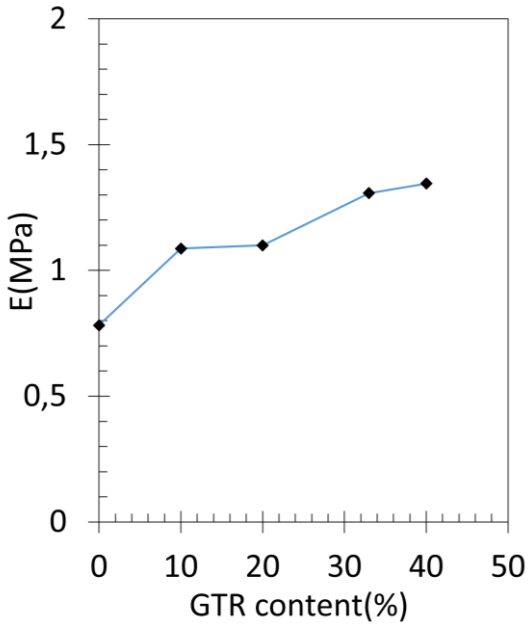


*Figure 40 Young's Modulus of NR/GTRx composites evaluated with MR model.*

We observe an increased tendency of the Young's modulus as function of the filler concentration (Figure 40), those underlining the reinforcement effect of the GTR particles presence. For higher deformations the experimental and the MR curves tend to diverge, as the model do not consider the phenomenon of SIC. Therefore, the onset of crystallization, can be deduced, investigating on the differences between the 2 curves. In particular, following the approach suggested by Candau[16] , we evaluated the difference in strain energy between the 2 curves as:

$$W_{gap}(\lambda) = \int_1^{\lambda} \sigma_{exp} - \sigma_{MR} \tag{27}$$

The integral is calculated with a numerical approach, using the Rectangular Approximation Method. Considering a number n of experimental points, the strain energy related to the single curve will be:

$$\int_1^{\lambda} \sigma = \int_0^{\varepsilon_{MAX}} \sigma = \sum_1^n \frac{(\sigma_{i+1} + \sigma_i)}{2} * (\varepsilon_{i+1} - \varepsilon_i) \qquad i = 1, \dots, n \tag{28}$$

The value of Energy Gap that we considered as the one related to the start of strain induced crystallization is of 0,01 MJ/m$^3$.

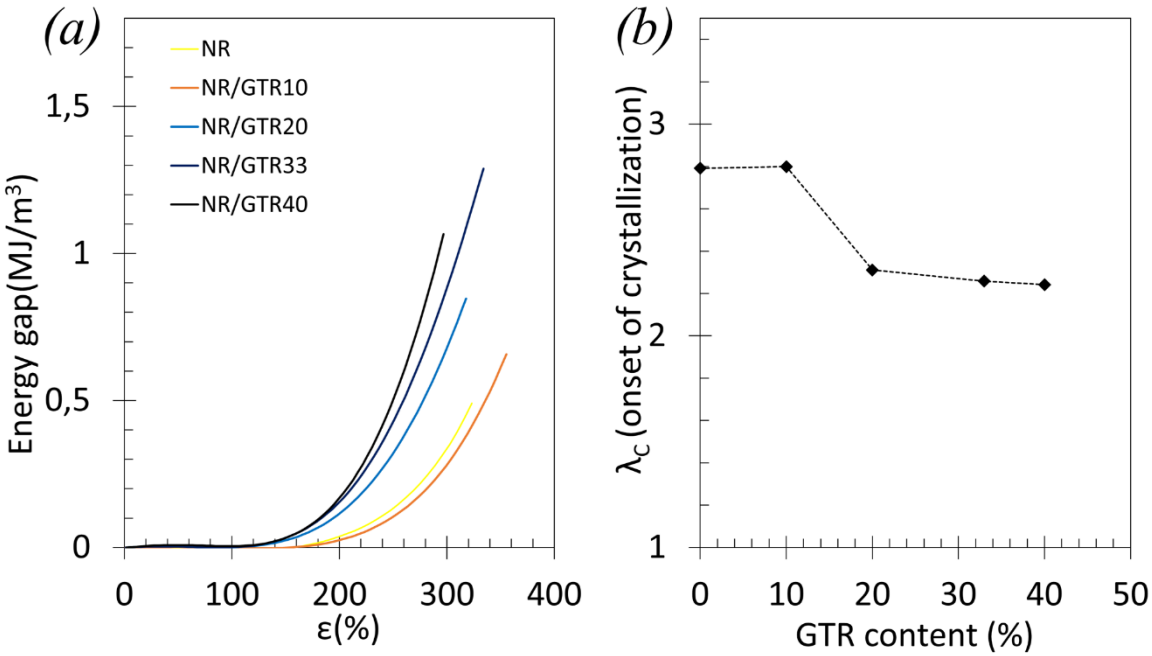


*Figure 41 a) Difference in strain energy between Experimental and MR model for NR/GTRx b) Onset of crystallization for NR/GTRx.*

Experimental results reported in Figure 41 shows that the onset of crystallization for NR and NR/GTR10 is very similar and happens at about at 200% deformation. This unexpected value can be attributed to the fact that the NR shows generally higher mechanical reinforcement than expected, and this behaviour is confirmed also by the loading cycles, which will be discussed in the section 5.3.2, where the NR sample is the only one surviving to the entire cycle. Another confirmation of this abnormal reinforcement come from the fact that in literature, vulcanized natural rubber shows the starting of crystallization for $\lambda \geq 3$[39], while here happens at lower λ. At the same time is possible that GTR particles in NR/GTR10 samples where not well-dispersed , those decreasing the reinforcement effect on the rubber. For higher GTR content we observe a gradual decrease of $\lambda_c$, suggesting the nucleating effect of GTR particles, as observed by Candau[40]. This effect is pronounced in NR/GTR40 and NR/GTR33 samples, where the onset of crystallization is observed at around 125% deformation.

Using the Mooney-Rivlin model is also possible to estimate the cross-link density, in the linear regime , as suggested by Vieyres[15]:

$$\nu_{MR} = \frac{(C_1 + C_2)}{RT\rho_{NR}\psi} \tag{29}$$

Where R=8,314 J/mol K, T is the temperature in K, $\rho_{NR}$ is the density of the natural rubber equal to 0,92 g/cm$^3$. Assuming a phantom model with tetrafunctional networks, the functionality will be f=4, and the parameter $\psi$ equal to:

$$\psi = \frac{f-2}{f} = \frac{1}{2} \tag{30}$$

We compared then the cross-link density of this model $\nu_{MR}$ with the one obtained from swelling experiments $\nu_{sw}$ (Figure 42).

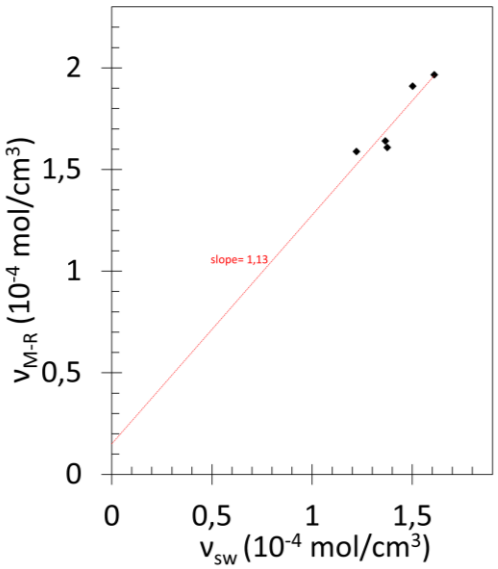


*Figure 42 Comparison between cross link densities, evaluated with MR constants and swelling experiments.*

The linear fit gives us a non-zero coordinate intercepts, meaning that the values of the density derived from MR are generally higher respect the one obtained from swelling behaviour. As suggested by Vieyres[15] this can be explained by the fact that in the swollen state we have much less effect of the physical entanglements, which will become un-active, those decreasing the crosslink density of the material. We observe that the linear fit is not very adapt to this set of data, and these differences can attribute to the assumptions of the model used for $\nu_{MR}$ , which assumes a phantom network, while $\nu_{MR}$ assume an affine one, and from some experimental uncertainty involving the swelling experiments.

### 5.1.3. Tensile tests: Effect of GTR content

As explained in chapter 2.2.3., the introduction of GTR particles in the rubber network can be treated as an introduction of rigid fillers, which effect is to enhance the local deformation of the NR's softer matrix. The increase in rigidity of the composites can be observed in Figure 43.

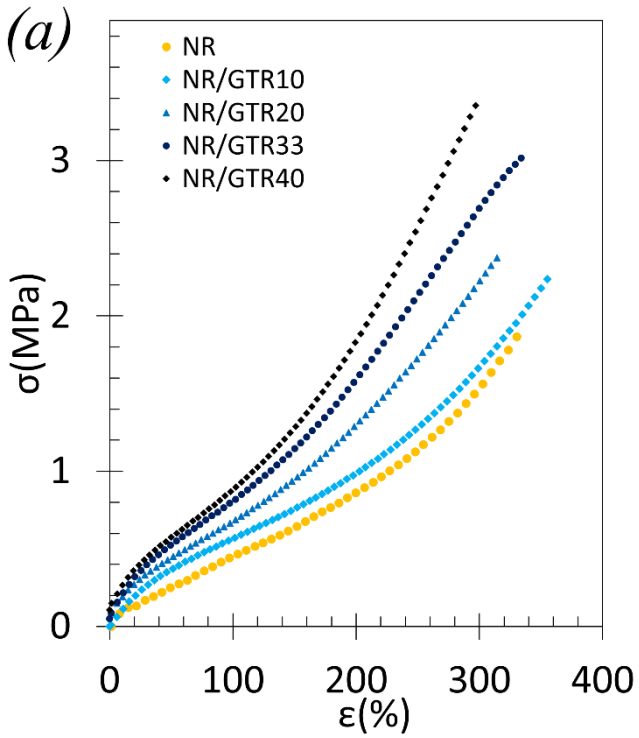


*Figure 43 Stress-strain curves at Tamb and V2=10 mm/min for different compositions.*

The experimental curves shows that the increase of filler contents cause an increase of the Young's Modulus in the linear part of the curves, for low deformations (<100%). Also, with higher contents of GTR, we observe a little decrease of the slope of the curve after the first linear elastic part. This decrease of the stress can be related firstly to the entropic effect, with the starting of the sliding of the chains, and for higher deformations, to the relaxation effect caused by the starting of the crystallization as explained in the section 2.1.3.

### 5.1.4. Tensile tests: Effect of strain rate

As observed in chapter 2.1, the increase of the strain rate causes an increase in the rigid response of the elastomer, as polymeric chains do not have enough time to slide and deform extensively. This expected behaviour is observed for both NR/GTR10 and NR/GTR20, with an increasing of the tangent modulus with the increase of the strain rate. Is interesting to observe that for both the samples, the increase is widely observable only for the highest strain rate 60 mm/min, while the mechanical response at 10 mm/min and 1 mm/min seems almost equal (Figure 44).

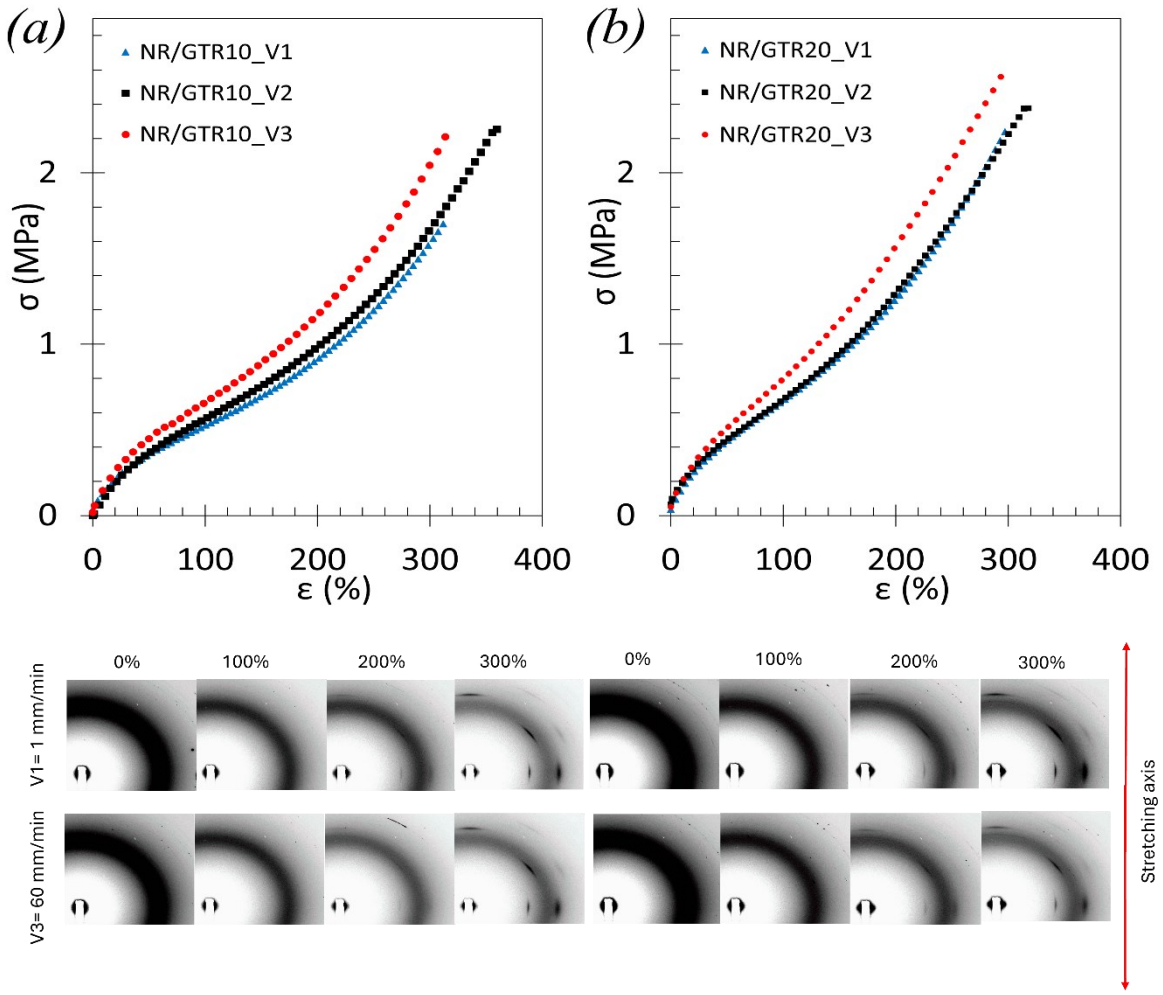


*Figure 44 a) Top: Stress strain curve for NR/GTR10 at different strain rates. Bottom: Diffraction patterns of NR/GTR10 at V1 and V3. b) Top: Stress-strain curve for NR/GTR20 at different strain rates. Bottom: Diffraction patterns of NR/GTR20 at V1 and V2.*

Thanks to X-ray diffraction patterns, showed in Figure 44, we notice that strain induced crystallization is activated already at 200% deformation, confirming what we deduced for the study of the onset of crystallization. At 200%, the crystalline halos of NR/GTR20 sample are more intense respect NR/GTR10, confirming that a higher filler content can promote the crystal formation and decrease the onset of strain induced crystallization.

### 5.1.5. Tensile tests: Effect of temperature

The elastic theories used for describing the stress-strain curves are based on purely entropic elasticity. With this description, the force needed to reach a particular stretching ratio, increases with the

increase in absolute temperature, as reported in equation (5). However, this is an ideal representation, and usually deviations are observed in the experimental data[14]. When discussing about the effect of the temperature, is important to consider both the role of viscoelasticity and strain induced crystallization. Similarly to what we observed for the strain rates, when the temperature is very low (-25/50°C) the atoms of the chains don't have enough energy to move and rotate, and the relative sliding of the chain is hindered, as we are approaching the glass transition temperature (-60°C). This cause a mechanical response that is more rigid respect higher temperatures, as observed in Figure 45(a).

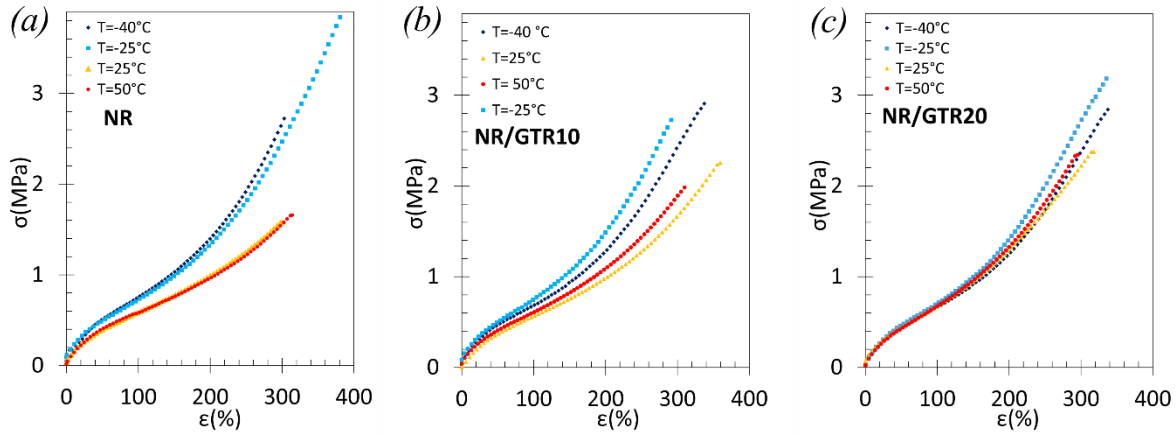


*Figure 45 Stress strain curves at different temperatures for a) NR b) NR/GTR10 c) NR/GTR20.*

Is interesting to notice that this phenomenon is less pronounced with NR/GTR composites, where the effect of temperature is less evident, as the curves have almost the same slope until 150% of deformation. Unfortunately, the abrupt stress upturn due to the reinforcement of the crystals is difficult to observe in our curves as it usually takes place at very high deformations (300-500%), which were not achievable in our experiments.

What we can observe, is the effect of the GTR content at a fixed temperature in Figure 46. At higher temperatures the filler's reinforcement take place, as NR/GTR composites present higher slope of the stress-strain curves, while for the lower temperatures, the effect of the fillers tends to disappear as the different samples tend to have very similar behaviour. The fact that NR sample show high rigidity can be justified by a possible over-reticulation of the pure natural rubber respect NR/GTR composites as previously discussed.

Diffraction patterns at fracture show the presence of crystalline phase for all the compositions and at all temperatures. The higher stresses are observed at -25°C, to which corresponds the highest intensity of the halos related to the crystals. As mentioned in the section 2.1.1., at -25°C there is the higher rate of temperature induced crystals, so it is possible that the higher rigidity can be also caused by an additional contribution of nucleation. However, we must remember that this mechanism possesses

very low kinetic: as reported by Toki[17], at -25°C , 27% of crystalline phase is formed after 2,5 hours , and these experiments were performed just in few minutes , so the main contribution to the crystalline formation still come from SIC.

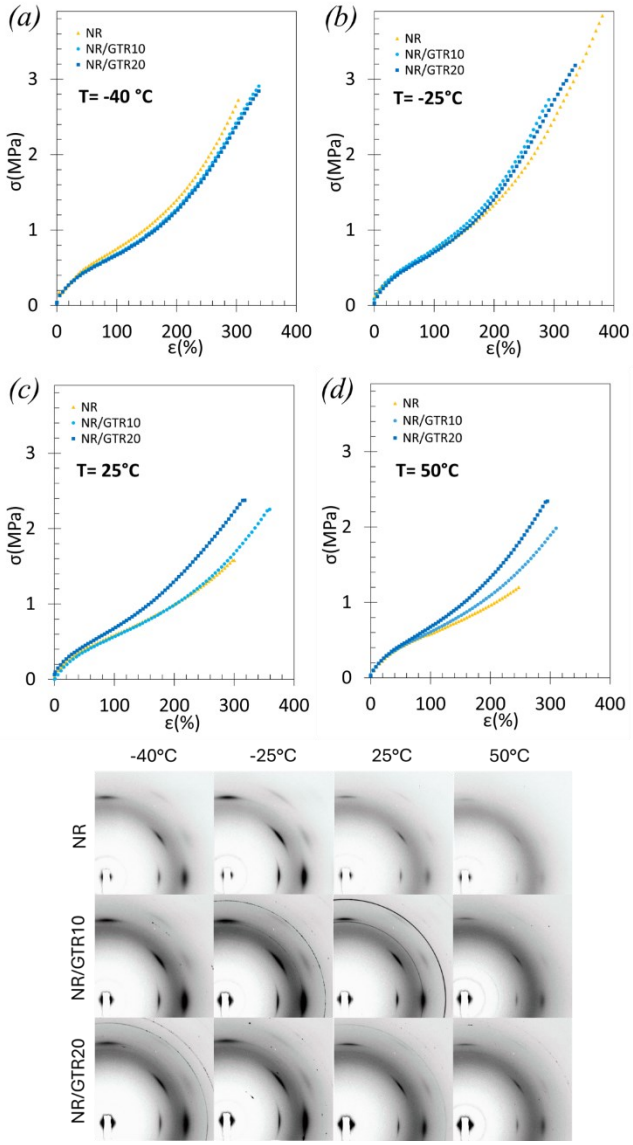


*Figure 46 Top: Stress-strain curves for NR, NR/GTR10, NR/GTR20 at different temperatures (a-d). Bottom: Diffraction patterns taken at fracture point.*

### 5.1.6. Cyclic tests: Hysteresis

The hysteresis is defined as the loss of energy due to loading and unloading cycles, where the energy is converted into heat. For measuring the dissipated energy, we evaluated the area between the loading and unloading curves for every sample, using the Rectangular Approximation Method as done in the section 5.1.1..

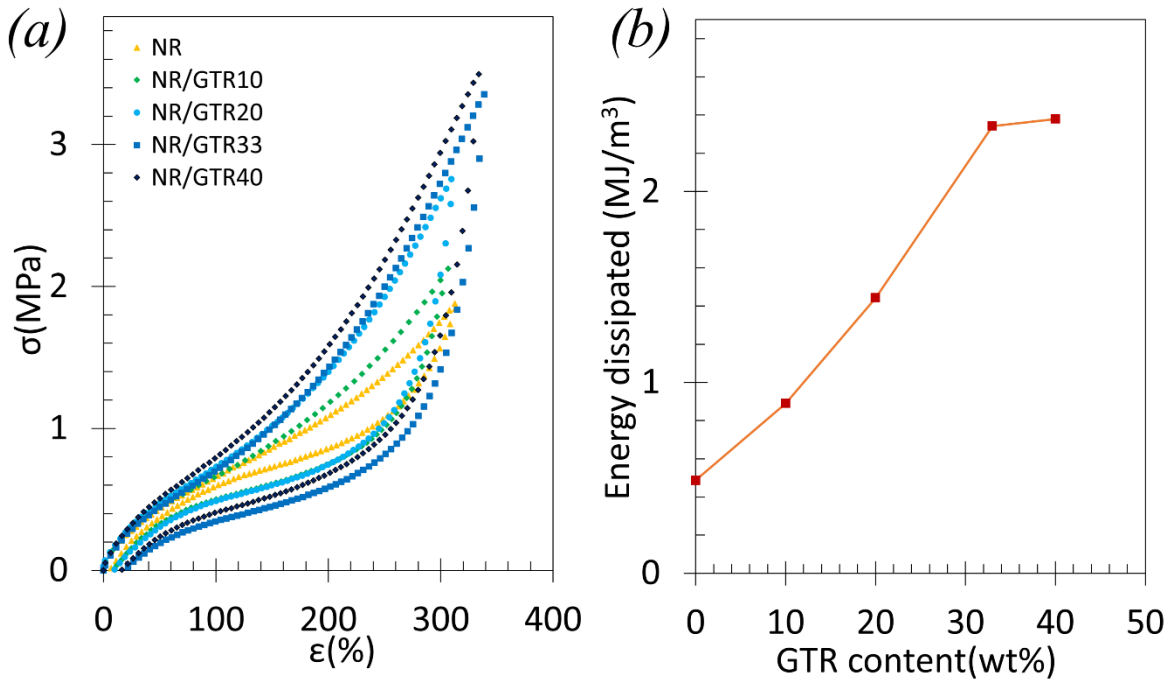


*Figure 47 a) Cyclic curves for NR/GTRx at V2=10 mm/min b) Energy dissipated in hysteresis for different compositions.*

We may notice from that, performing a single cycle, we cannot be sure that , when the material return to a null stress even the deformation energy return to 0, as it can be possible that the zero stress is obtained as a balance between compressive and tensile residual stresses and the best way for evaluating it, would be in steady state conditions with different cycles, as reported by Ferry[7]. For our purpose we will neglect this aspect, as the results still give us important information. From Figure 47, a gradual increase in the hysteresis with the increase of fillers up to 33% of GTR is noted, reaching a plateau for higher concentration. Comparing NR with NR/GTR33 composite we observe an increase of almost 5 time of the hysteresis. As reported by Rault[41] , the mechanical hysteresis for high deformations (ε>1) is an effect of strain induced crystallization and not from viscoelastic effects. Therefore, the energy loss can be related to the melting of the crystals when the material is un-loaded. So, higher energy losses can be attributed to the melting of a higher amount of crystalline phase for the NR/GTRx composites respect the NR. The plateau at high filler contents can mean that for high concentration of GTR we may reach point where we can't have an increase in crystalline volume but only in the number of crystals, as the growth of the crystallites will tend to be blocked by both the GTR particles and cross-links presence.

### 5.1.7. Cyclic tests: Thermal cycles

The only sample survived to the entire loading and thermal cycle is the pure NR, which is reported in Figure 48. This high resistance can be a confirmation on what mentioned above that the natural rubber

possesses very high reticulation and physical entanglements. This observation can be also in accordance with the fact that NR presents the higher onset of crystallization, as it is possible that a higher number of cross-links obstacles the alignment of long chains, and consequently the formation of crystals.

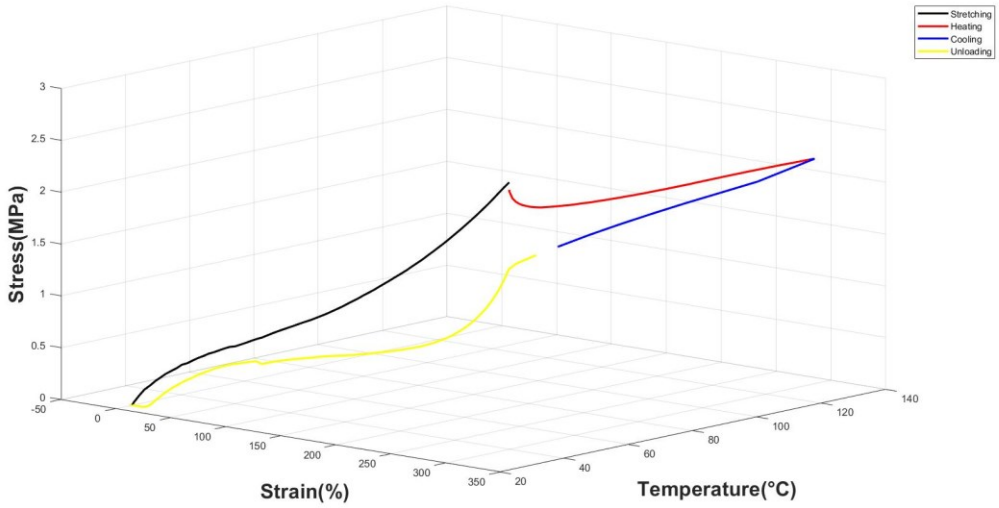


*Figure 48 3D Loading and thermal cycle: Stretching, Heating, Cooling, De-stretching.*

The stretching was performed until the maximum deformation achievable by the Stretcher, and for the different samples the range of maximum deformations was between 340 and 355%. In this condition, after the stretching stage, the sample will have developed some crystalline phase. Keeping the constant strain, the chains will remain aligned, while the increase of the temperature will increase the vibration of the atoms of the chains, and consequently the possibility of having degradation and rupture of the cross-links and of the C-C bonds of the backbones.

### 5.1.8. Cyclic tests: Fracture of NR/GTR during thermal cycles

Is interesting to notice that NR/GTR samples fractured during the heating stage at maximum deformation. In Figure 49 the temperature of fracture of the different samples is reported. Respect the NR, which resisted until 120°C, the NR/GTR10 broke at 95°C showing lower mechanical resistance and this is probably due to a bad interface between NR and GTR. When the amount filler increases also the temperature of fracture increases. This phenomenon can be due to the higher nucleating effect of the GTR particles, which increases the amount of crystalline phase and consequently the thermal energy needed for the melting of the crystals r. This is confirmed by the diffraction pattern which shows higher crystalline halos with higher amount of GTR. Also, the high concentration of filler can play an important

role in avoiding crack propagation, as cracks can deviate their path when they encounter the particles, so the material is able to dissipate more energy.

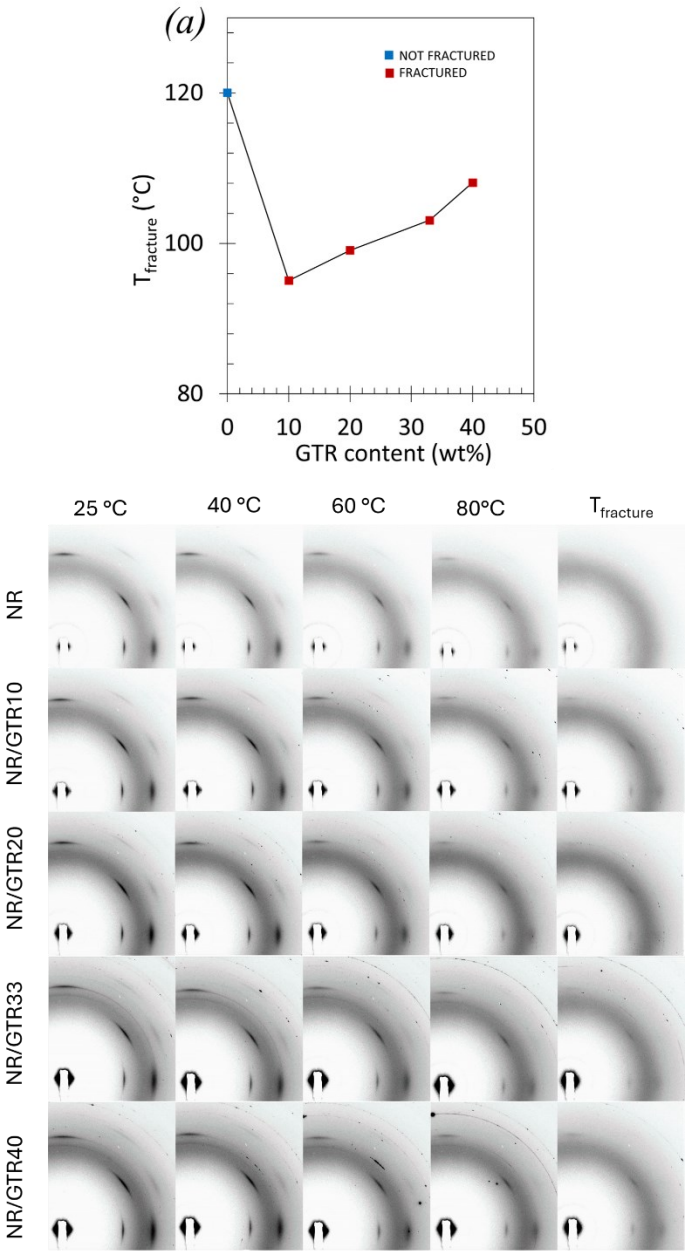


*Figure 49 Up: a) Fracture temperature at different composition during heating at fixed deformation. Bottom: Diffraction images at different temperature until fracture.*

### 5.1.9. Fracture analysis of NR/GTR with SEM.

To further confirm what deduced in the previous discussion, we performed SEM analysis for the different blends with different magnification to understand the fracture mechanisms. From Figure 50

we observe already that the higher presence of fillers increases the rugosity of the samples, which is strictly connected with the decohesion in the areas of the particles before fracture.

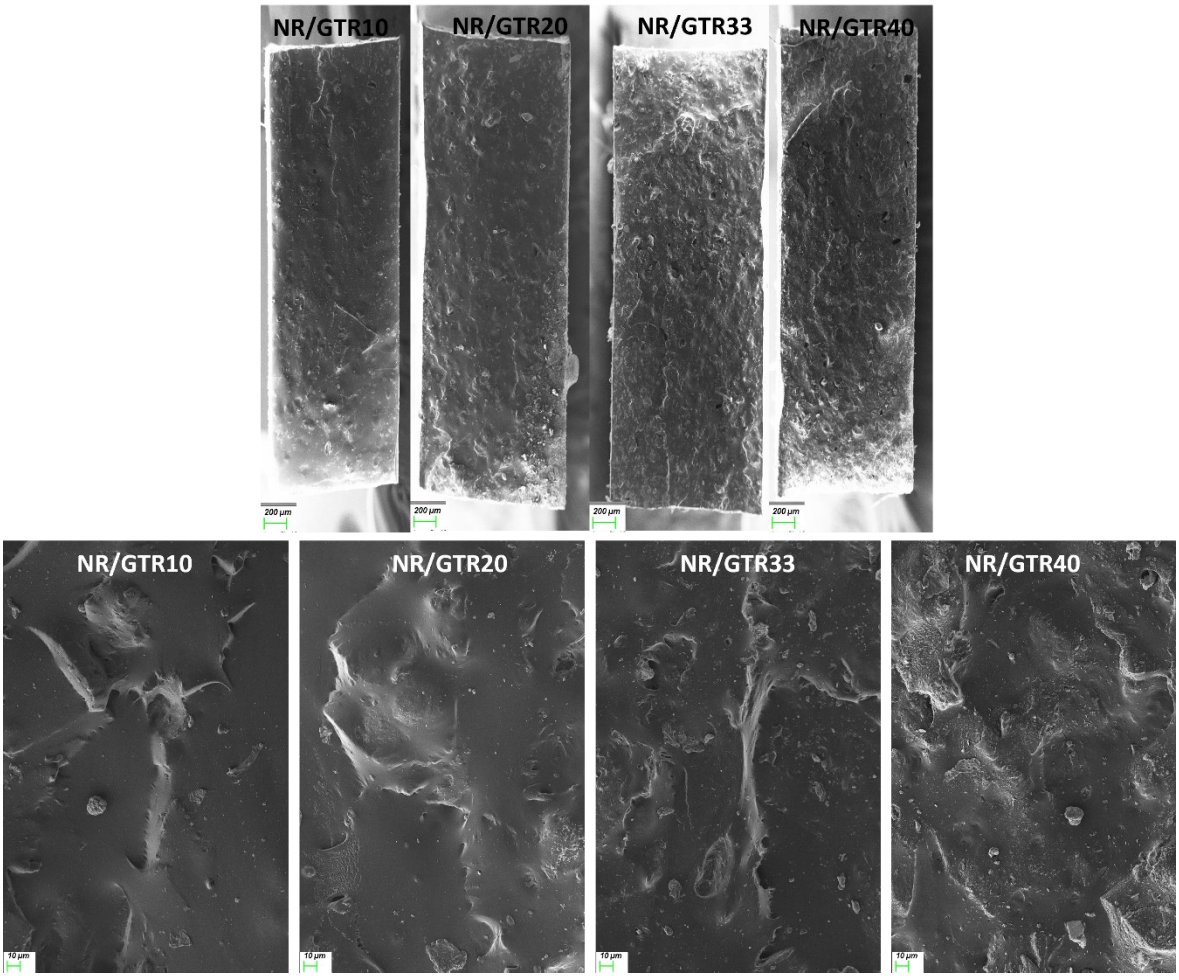


*Figure 50 SEM images of the fracture surfaces of NR/GTR samples. Up: 25X magnification Bottom:300X magnification.*

For the particles that remained attached to the matrix is possible to observe their presence as single particles, for the smallest one, and in the form of agglomerates in the biggest one, as observed for NR/GTR20 (Figure 51).

The lines of the cracks shows that cracking can happen both with high propagation as observed in NR/GTR10 at 300X and NR/GTR33 at 1000X, but also with local, which is observable for all the blends. This means that at 33% of filler we didn't still achieve an efficient deviation of the crack propagation; while at 40%, where these lines are not present, it suggests a higher efficiency of the material in blocking the crack path. The higher content of filler ensures a higher number of crack with different direction and with shorter path.

All samples show areas where the matrix is still highly stretched near the particles, confirming their effect in enhancing the local deformation. Is interesting to see in the NR/GTR20 the presence also of micro-cavitation with fibrils and voids, which are unexpectedly oriented in the transverse direction respect the stretching one.

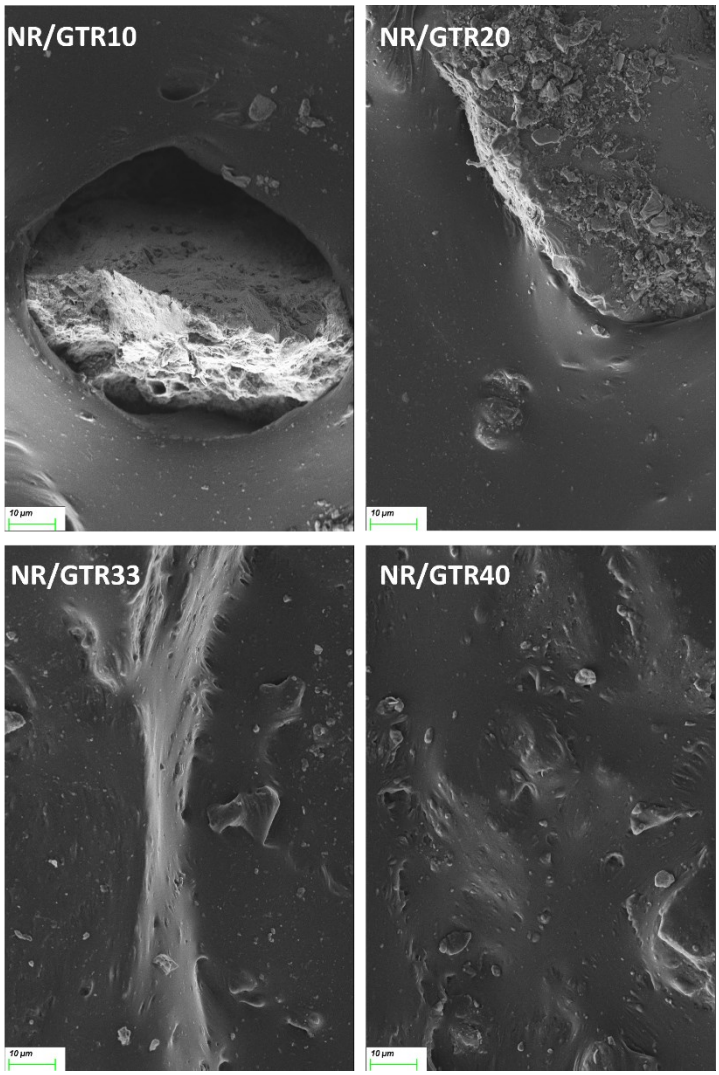


*Figure 51 SEM images of NR/GTR at 1000X magnification.*

Fibrils due to a strain enhancement are wide observable in NR/GTR40 sample as shown in Figure 52. Is interesting to notice that the diameter of the fibril seems strictly related to the particle size responsible for the stress concentration. This can confirm that smaller particles will increase the amount of matrix subjected to strain enhancement and consequently improving the mechanical properties of the NR but especially allowing the inhibition of the lateral crack growth.

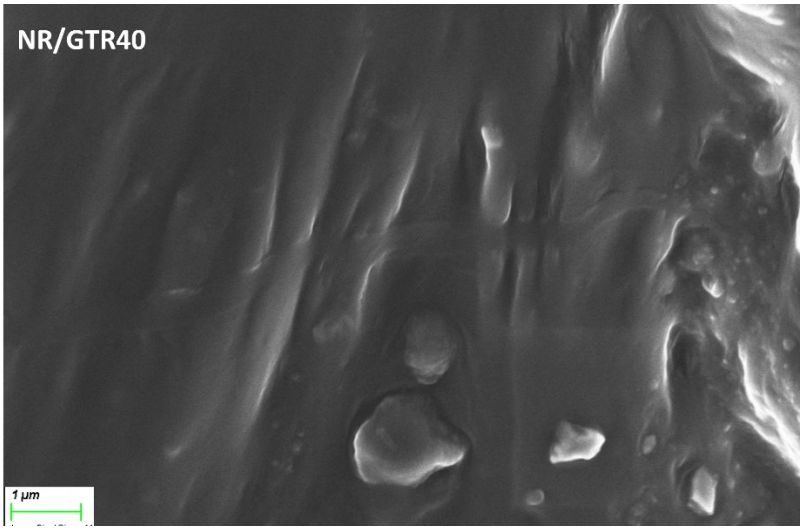


*Figure 52 SEM image of NR/GTR40 at 10000X magnification.*

## 5.2. Devulcanization of GTR particles

### 5.2.1. TGA of GTRs

In Figure 53 the weight loss curves are represented for the different devulcanization powers. The first abrupt decrease of weight corresponds to the range of temperature between 200 °C and 450 °C, and it can be associated to the evaporation or decomposition of the oil and other organic additives present both in GTR and NR[31]. From 850 °C when the environment condition is changed to $N_2/O_2$ the thermo-oxidation of CB happen, with a loss in mass of the 5-10% of the sample. The percentage of Carbon remained after the test is between 25% and 35%.

We observe that for a devulcanization time of 10 minutes for 400 and 640 W we have much less organic compound respect the other set of time and powers, and this is a confirmation on what obtained experimentally from the devulcanization process, as for these samples we had development of smoke and burning of the GTR, reaching temperatures higher than 220°C. This means that a good amount of the organic compounds already decomposed or evaporated during the devulcanization process before performing TGA.

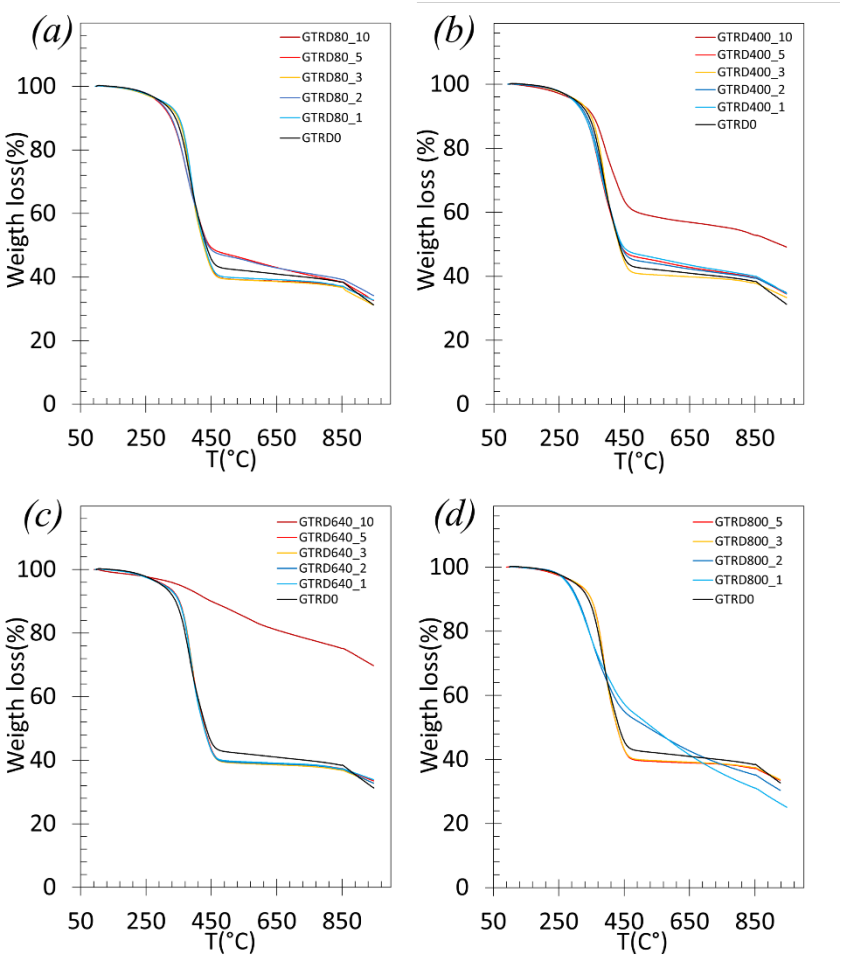


*Figure 53 TGA curves for GTRD at different powers: a) 80W b) 400W c) 640W d) 800W*

We observe a particular behaviour also for the samples treated at 800W for 1 and 2 minutes, where the decomposition of the organic materials start at lower temperatures: the speed of decreasing is lower respect the other samples of the same power and we do not observe the plateau between 450°C and 850°C, meaning that the loss in weight happen more gradually in a higher temperature range. This is reflected in the CB content, as from Figure 54, we observe that for these 2 samples we have the lower amount of CB, meaning the presence of more organic compound. A possible explanation of the decrease of CB content can be that, during heating at this power, the C can be released from the CB aromatic structure and form more volatile compounds which degrade a temperature higher than 450°C.

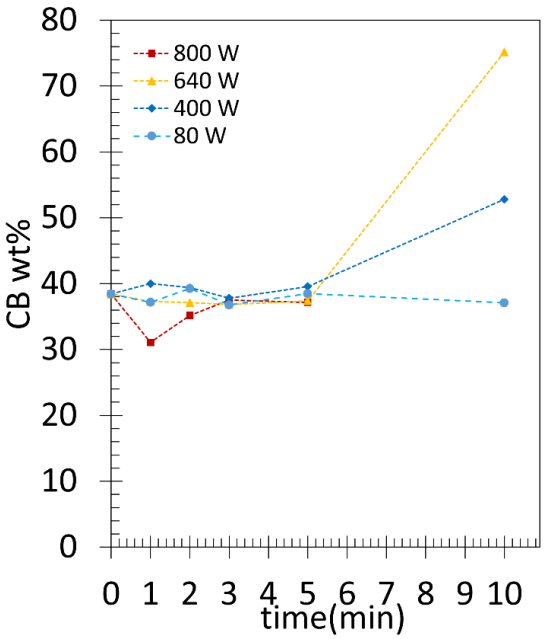


*Figure 54 CB content of GTRD at different powers.*

### 5.2.2. Swelling of GTR particles

Swelling test were performed to evaluate the crosslink density of the GTRD after devulcanization, which are reported in Figure 55. The trends are of difficult interpretation, as apart from the 400 W samples, at 1 minute we obtained a much higher cross-link density for all the other powers, compared to the non-devulcanized powder, which is difficult to explain, especially for 80 W.

However, there is a common tendence to decrease the cross-link density for time of exposure higher than 2 minutes, meaning that there is sufficient energy to have bond breakage. This decrease is less pronounced for the lower powers, meaning that we probably didn't achieve enough degree of devulcanization. This can be observed especially for the lower power 80 W, where the cross-link density has very low variations for all the times, and we find further confirmations by the measure of the T of the samples, which we will see in the next section.

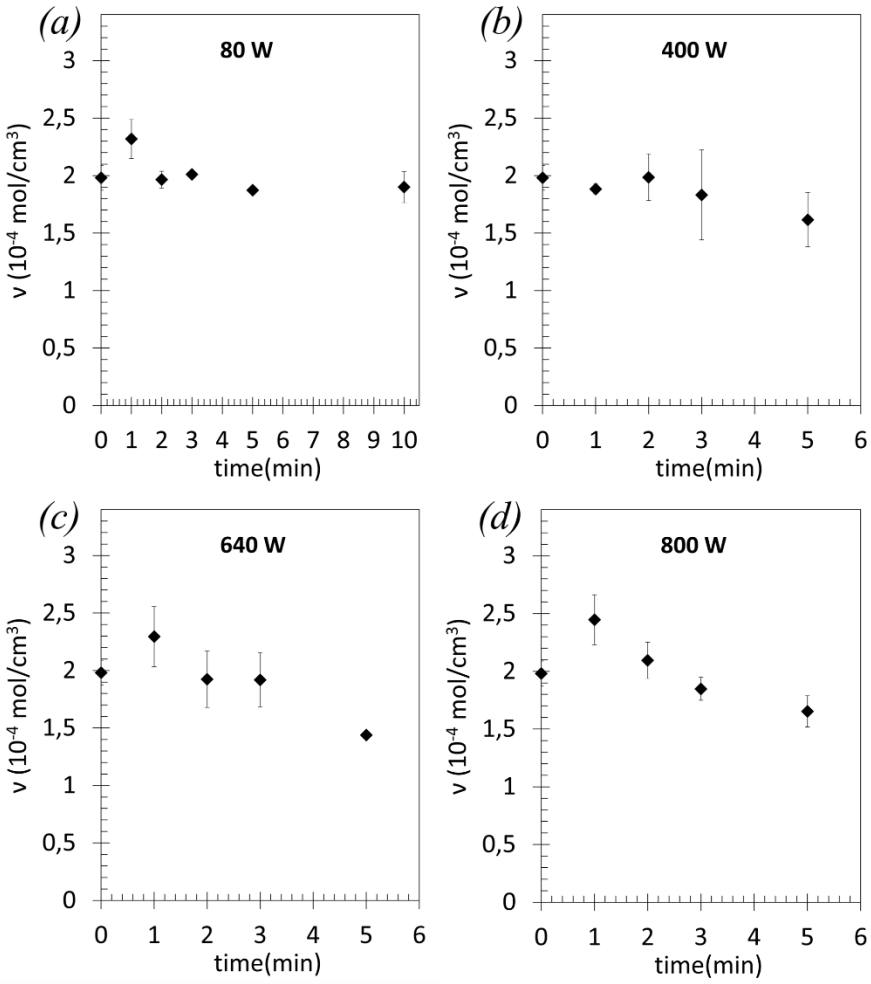


*Figure 55 Cross-link density as function of devulcanization time for different powers.*

For 400 W the trend of decreasing start to be more pronounced, but still not sufficient for achieving enough degree of devulcanization. For 640 and 800 W the trend is similar. At these powers we reach much higher temperatures, and the particles can absorb enough energy to have re-vulcanization, but also there can a possible rupture of the double C=C bonds of CB. The competitiveness of devulcanization and re-vulcanization processes influences sensibly the decrease in cross-link density. 640 W treated samples achieved lower v, suggesting that this power could be be the more suitable for this process.

Is important to notice that the standard deviation of the data for the higher powers is high, which is probably the main reason connected with the difficulty of observing trends that are more in accordance with the literature and with the physical mechanisms controlling this process.

### 5.2.3. Temperature of the devulcanized GTR particles

In Figure 56, the temperature achieved by all the samples after the devulcanization process is reported. For the intermediate powers 400W and 640 W we observe a gradual increase of the temperature respect the devulcanization time, suggesting a possible proportionality between these 2 parameters. However, for 800W, we see a higher increase of T for devulcanization time of 1 and 2 minutes, and a much lower one for higher radiation time which is not in accordance with swelling tests. A similar behaviour, but more pronounced, is observable for the lower power 80W, where the increase in T is very low until 3 minutes, for then achieving a stable value for higher time. In this case the trend of the temperature is very similar to the one observed in the swelling test.

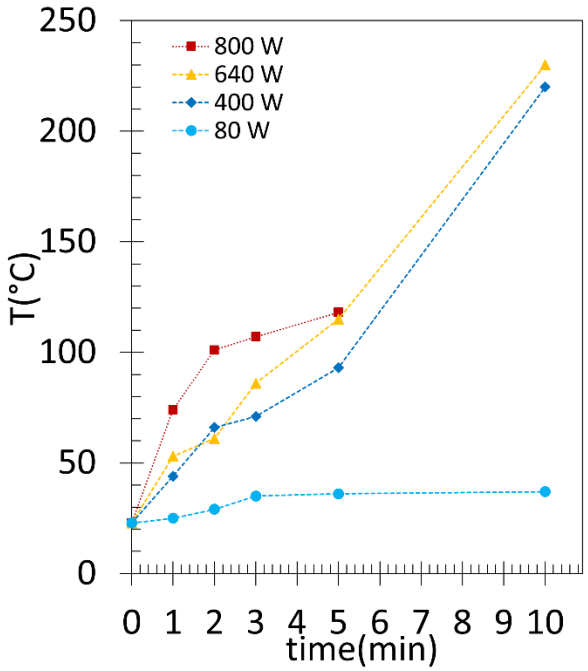


*Figure 56 Temperature of the samples after devulcanization.*

So ,the temperature of the sample could be an indicator of the amount of devulcanization performed in the material as reported in other works[31], but it cannot be extended to all the sets of microwave powers and times , because if we compare these results with the cross-link densities of the materials , there is no strong correlation between these 2 parameters. For a time of 10 minute at 640W and 400W we have burning of the rubber, to which is associated a high increase in temperature which is almost the double respect 5 minutes.

The evaporation of some organic compounds starts already from temperatures higher than 100°C, as we observed the development of smoke in the samples that reached this temperature, so mainly the

GTR treated at 800 W for times higher than 2 minutes. This is in accordance with the TGA, as these samples present higher CB respect the lower times.

### 5.2.4. FTIR spectroscopy

We performed FTIR spectroscopy to have more information regarding the rupture of S-S, C-S and C-C bonds. Their amount is evaluated respect the C-H bonds and the data are reported in Figure 57.

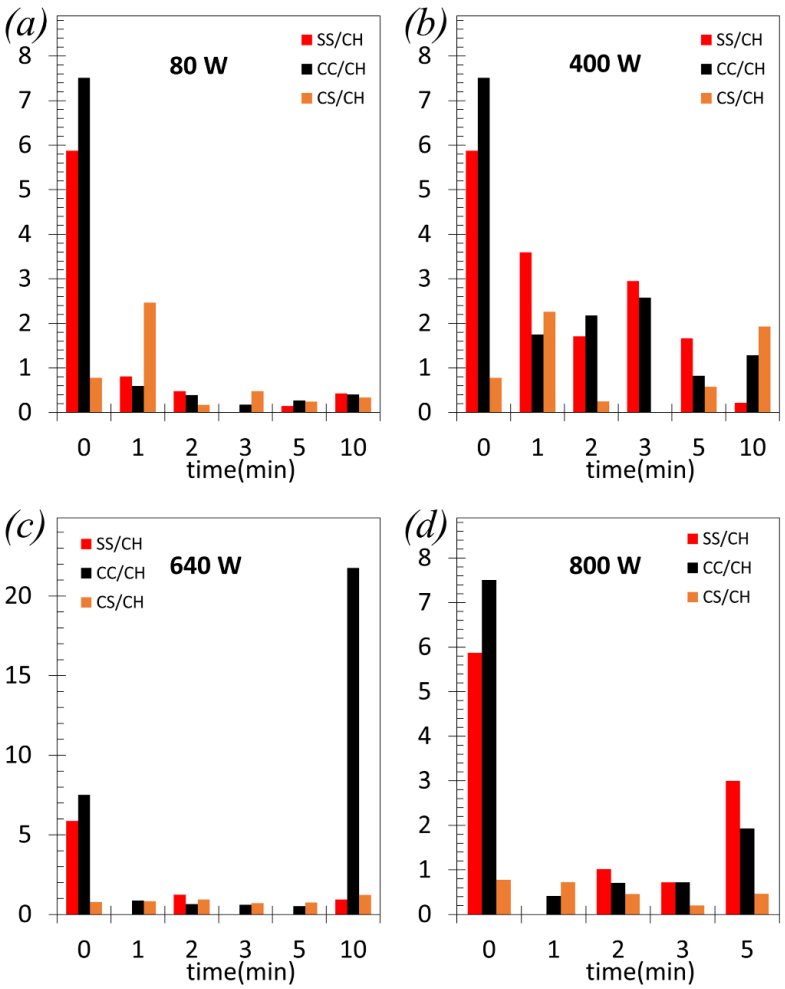


*Figure 57 Ratio of the bonds evaluated from FTIR spectroscopy.*

The signals of C-S and S-S were difficult to detect for many samples and for others were indetectable, especially for the samples treated for 3 and 5 minutes and at 640W. This is in accordance with the cross-link density measurements, as for these devulcanization times we have the lower values of v for all the powers, meaning that the scission of the bonds could be completely achieved for these blends.

The higher values of cross-link density obtained for 1 minutes are confirmed by the presence of a higher amount of C-S, which were not broke during the devulcanization, apart for the 640 W samples.

For the samples which undergone to burning at 10 minutes, we observe an increase in the C-C content which is in accordance with a higher presence of CB as observed in the TGA measurements. C-C bonds decrease rapidly for the short times, to generally increase for higher devulcanization times, suggesting a possible reformation of these bonds, for which we still not have a physical explanation.

## 5.3. Elastocaloric properties of NR/GTRD blends

### 5.3.1. Tensile tests on NR/GTRD800 blends

We performed tensile test until rupture with strain rate of 3000 mm/min for the NR/GTRD blends devulcanized at 800 W for 1,2,3 and 5 minutes, as this power is one of the most investigated in literature for microwave devulcanization and the decrease in cross-link density seem more evident respect the other powers. NR/GTRD800 blends were vulcanized, so GTR particles undergo to a re-vulcanization process, that after the first devulcanization with microwave, should improve the matrix/filler interface with the creation of new cross-links.

Tensile test, reported in Figure 58 shows the mechanical resistance of the different blends compared to the evolution of the temperature. The blend which shows higher ΔT during stretching is the one treated with 2 minutes, and the one that showed higher stress at fracture is the one treated with 1 minutes, which is in accordance with its higher cross-link density. Non devulcanized GTR seem to have a higher reinforcement effect respect the devulcanized one, so it is possible that the re-vulcanization process was not achieved as expected.

The difference in temperature of the materials during heating, seem not correlated with the time of devulcanization, as the values are quite stable around 9°C, with a maximum ΔT of 12°C experienced by NR/GTRD800_1.

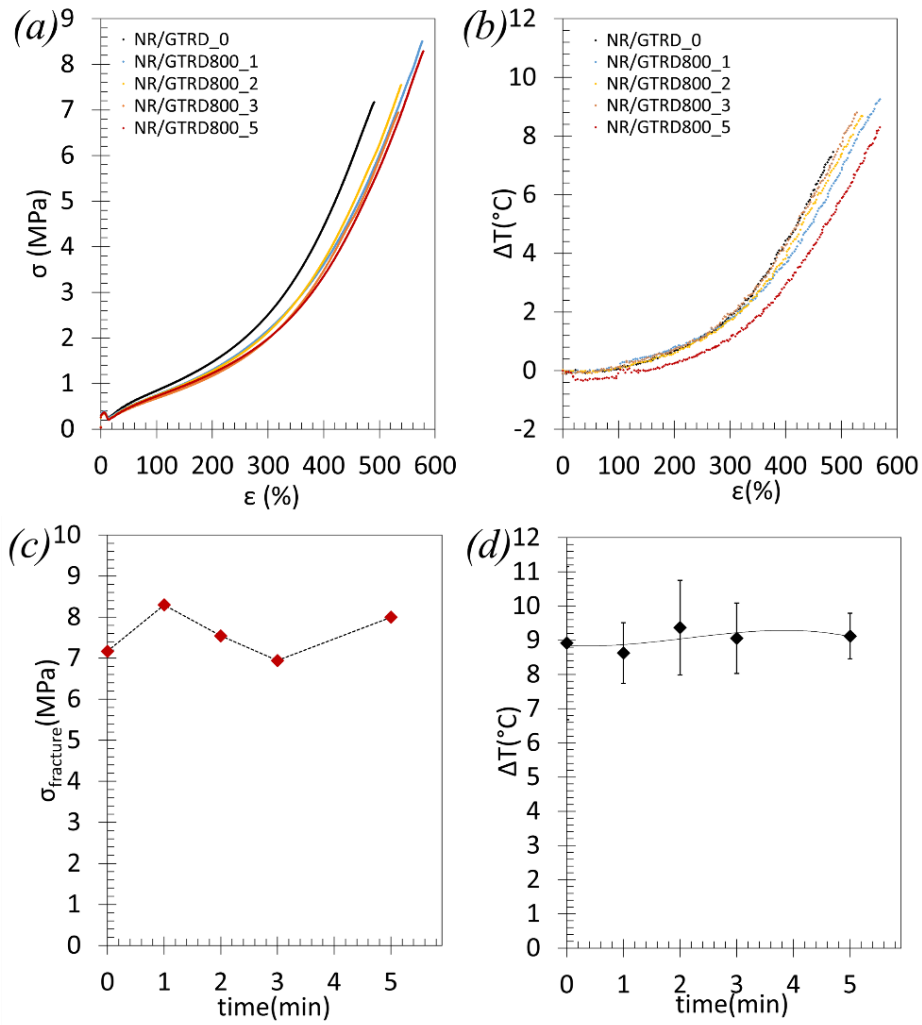


*Figure 58 Tensile tests for NR/GTRD800: a) Stress-strain curve b) Difference in temperature respect the deformation c) Stress at fracture respect devulcanization time d) Maximum difference in temperature respect devulcanization time*

### 5.3.2. Cyclic tests of NR/GTRD800 blends

The same blends were tested in cyclic test until a maximum deformation of 500%. During stretching, the materials increase their temperature, while during unloading they cool down below the starting temperature. In Figure 59 stress strain curves together with ΔT are reported. The relaxation phase after loading is fundamental, as it permits the completion and the stabilization of the strain induced crystals formed during heating, and that will be responsible for the successive cooling[42].

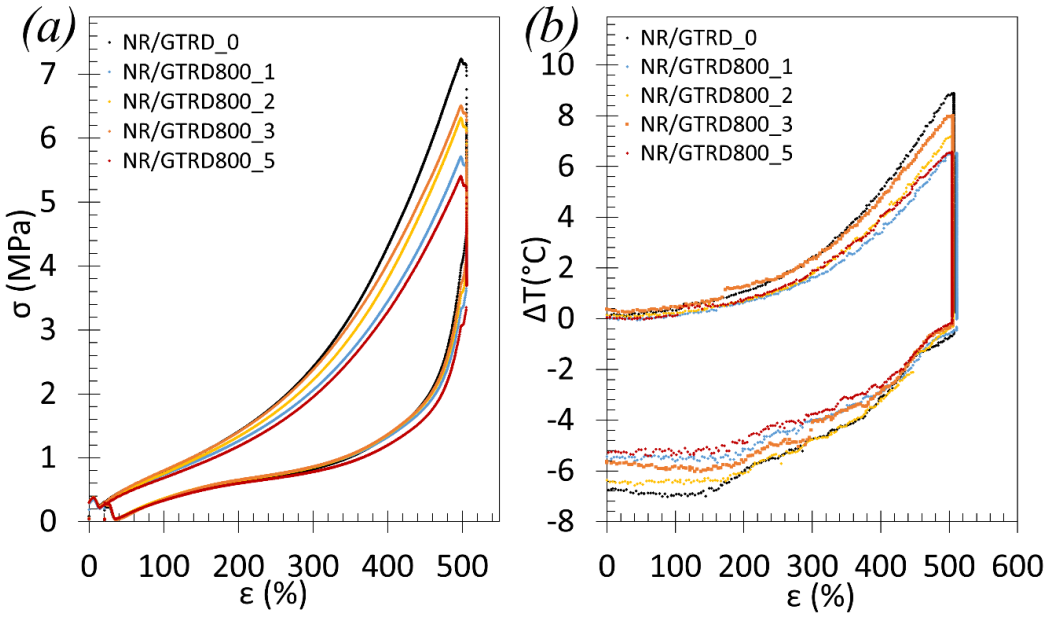


*Figure 59 Cyclic tests for NR/GTRD800: a) Stress-strain curves b) Difference in temperature respect deformation.*

Even in these tests there is the confirmation that NR/GTRD0 have better reinforcement respect the other materials, but in this case, it possesses also higher ΔT during heating. We define $\Delta T_{max}$ as the maximum difference in temperature experienced during heating, and $\Delta T_{min}$ as the maximum difference in temperature experienced during cooling. Starting from these 2 values we can than define an overall difference in temperature experienced by the material during the entire cycle as:

$$\Delta T_{span} = |\Delta T_{max}| + |\Delta T_{min}| \quad (31)$$

The values of these parameters are displayed in Figure 60, together with mechanical energy dissipated by the material $E_m$, calculated using the same method reported in section 5.1.2. with equation (28). The heat dissipated is related to the fact that crystallization and melting of the latter is not a symmetric process[42]. We remember that, as these blends contain 20 phr of GTR and the average content of CB in the GTR is around 38%, the weight fraction of CB in the NR/GTRD800 should be around 8%, which is probably still a low content for having a sensible improvement of the thermal conductivity of the NR, and consequently a good heat dissipation of the material during the cycle. Blends with higher percentage of filler should tested to observe the influence of CB in the elastocaloric properties as a thermally conductive filler achieving a higher heat dissipation.

From the graphs in Figure 60 is evident that in the NR/GTRD0 sample we observe the higher difference in temperature, while the lower difference is observed for NR/GTRD800_1 and NR/GTRD800_5. In this case, even if the GTRD800_1 showed higher cross-link density, it shows lower ΔT respect the other

materials, meaning that the crystalline phase formation is probably not efficient as for the other blends.However, the lower ΔT of NR/GTRD800_1 and NR/GTRD800_5 is compensated by a lower heat dissipation, and this will affect the final performance of these blend, as we will see in the next section.

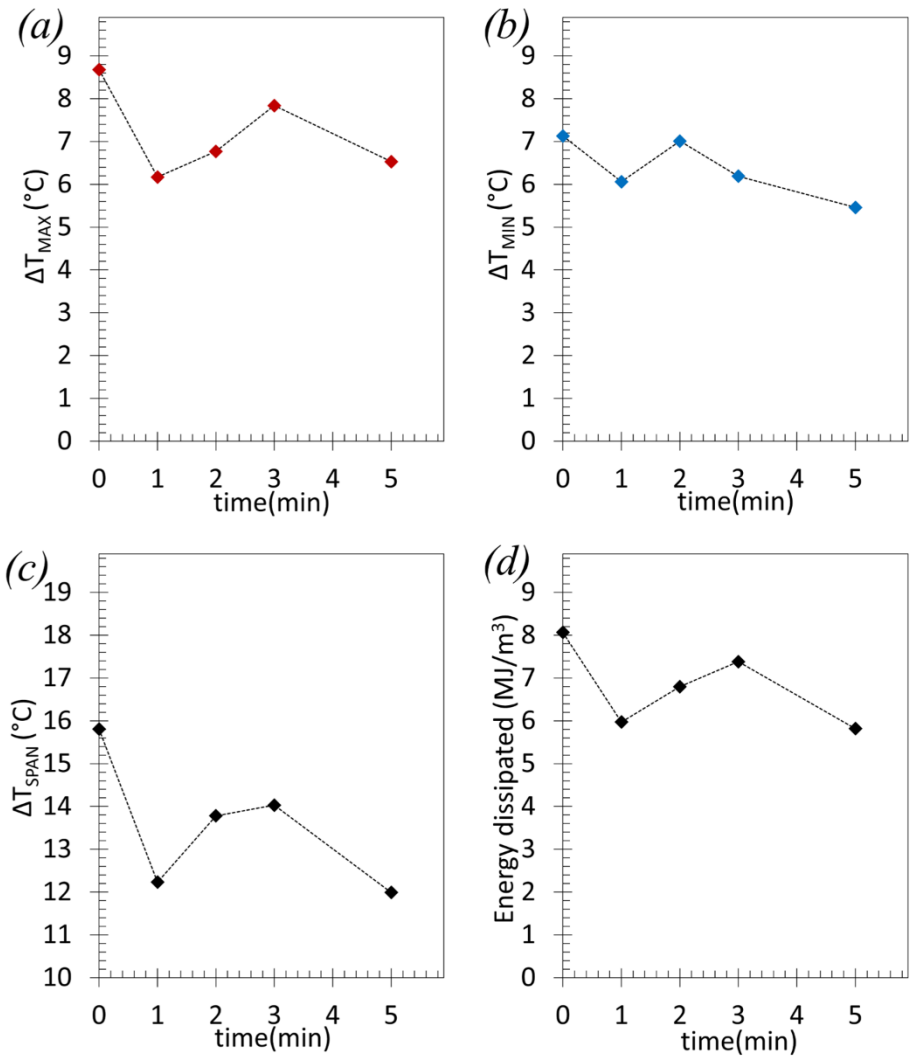


*Figure 60 Cyclic test for NR/GTRD800: a) Maximum difference in temperature during heating b) Maximum difference in temperature during cooling c) Maximum difference in temperature during the entire cycle d) Mechanical energy dissipated during the entire cycle*

### 5.3.3. Coefficient of performance of NR/GTRD800 blends

Is possible to have an estimation of the efficiency of these blends for potential heating/cooling applications, calculating a coefficient of performance of the materials $COP_{mat}$ which is defined as:

$$COP_{mat} = \frac{Q^+ - Q^-}{E_m} \quad (32)$$

Where $Q^+ - Q^-$ is the amplitude of heat exchanged during heating and cooling and $E_m$ is the mechanical energy dissipated, that we already introduced.

A simplified expression can be used, assuming fully adiabatic conditions, which in this case can be assumed due to the high strain rate, and it is expressed as:

$$COP_{mat} \approx \frac{\rho C \Delta T_{span}}{E_m} \quad (33)$$

Where ρC is the product of the density and the heat capacity of the material[43], which is equal to 1,75 $MJ/m^3K$.

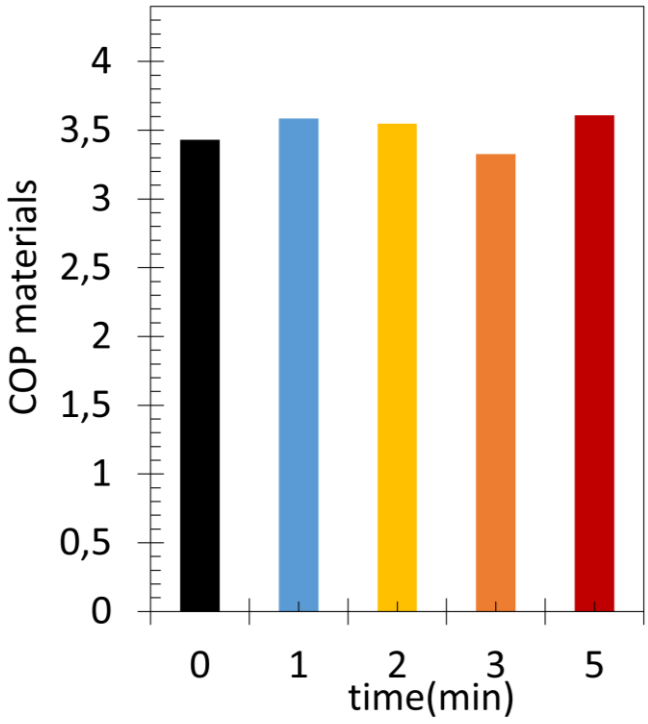


*Figure 61 COP of NR/GTRD800 at different devulcanization times.*

From the values calculated for the different blends (Figure 61), we observe that the higher $COP_{mat}$ is obtained for NR/GTRD800_1, equal to 3,58, and NR/GTRD800_2, equal to 3,6 . Even if these materials showed lower $\Delta T_{span}$, they perform better as they have less energy dissipation. NR/GTRD800_1 showed same ΔT in tensile and cyclic test (12°C).

However, we observe that the values obtained for the other materials, even if lower, are very similar, with lowest COP equal to 3,33, for NR/GTRD800_3. The fact that 3 blends with devulcanized GTR performed better than the one with non-devulcanized GTR means that the devulcanization process can have a positive effect on the elastocaloric properties of NR/GTR blends.

In order to employ these materials for real heating/ cooling systems, they will need to resist to a high number of cycles without rupture, and for this reason a study on the fatigue behaviour of these blends will be fundamental to understand their true potential.

# Conclusions

The aim of the work was to find an efficient method to recycle the waste of rubber coming from tyres (GTR), incorporating the material in natural rubber matrixes, to create blends with high added value for heating and cooling applications.

We first investigate the effect of the GTR on the ability of the natural rubber matrix to crystallize under strain. In situ WAXS experiments confirmed the expected effect in SIC of the filler introduction in NR matrix. With increase in GTR content a decrease in the onset of crystallization is observed during tensile loading. The effect of the GTR on mechanical reinforcement is more pronounced at temperatures at and above room temperature. Also, the GTR particles had positive effect in increasing the fracture temperature of the NR/GTR blends during heating at fixed extension, suggesting their capability in deviating the crack propagation.

As an intent to optimize the interfacial properties between the natural rubber matrix and the GTR particles, the GTR particles have been devulcanized and the blend further re-vulcanized using sulphur. Microwave devulcanization of GTR particles had variable effect in their cross-link density, depending on the time and the power used. The decrease in cross-links is more pronounced for devulcanization time higher than 2 minutes, and for the highest output energies evaporation and decomposition processes were observed. The increase in temperature of the particles seemed not correlated with the degree of devulcanization of the material.

The elastocaloric effect of the NR/GTRD blends was studied during tensile cycles at high strain rate by using the infrared thermography technique. Introduction of GTRD devulcanized with 800 W in NR matrix changed sensibly the elastocaloric properties of the blend, with different effects depending on the type of loading. From tensile tests we didn't observe a strong effect of the devulcanization in the difference in temperature experienced by the blends, even if the NR/GTRD800_1 experienced the highest $\Delta T$ of 12 °C.

In cycling loading, NR with non-devulcanized GTR showed higher $\Delta T$ (15°C) respect the other blends. However, the higher amount of heat dissipated lowered its efficiency as material for heating and cooling systems. The higher coefficient of performance was observed for NR/GTRD800 treated at 1 and 5 minutes, showing potential improvement thanks to the devulcanization process.

# BIBLIOGRAPHY


(1) Surya, I.; Maulina, S.; Ismail, H. Effects of Alkanolamide and Epoxidation in Natural Rubber and Epoxidized Natural Rubbers Compounds. *IOP Conf. Ser. Mater. Sci. Eng.* **2018**, *299*, 012061. https://doi.org/10.1088/1757-899X/299/1/012061.

(2) Tanaka, Y. Structural Characterization of Natural Polyisoprenes: Solve the Mystery of Natural Rubber Based on Structural Study. *Rubber Chem. Technol.* **2001**, *74* (3), 355–375. https://doi.org/10.5254/1.3547643.

(3) Bhowmick, A. K.; Stephens, H. *Handbook of Elastomers, Second Edition,*; CRC Press, 2000.

(4) Amnuaypornsri, S.; Toki, S.; Hsiao, B. S.; Sakdapipanich, J. The Effects of Endlinking Network and Entanglement to Stress–Strain Relation and Strain-Induced Crystallization of Un-Vulcanized and Vulcanized Natural Rubber. *Polymer* **2012**, *53* (15), 3325–3330. https://doi.org/10.1016/j.polymer.2012.05.020.

(5) Akiba, M.; Hashim, A. S. Vulcanization and Crosslinking in Elastomers. *Prog. Polym. Sci.* **1997**, *22* (3), 475–521. https://doi.org/10.1016/S0079-6700(96)00015-9.

(6) Kruželák, J.; Sýkora, R.; Hudec, I. Peroxide Vulcanization of Natural Rubber. Part I: Effect of Temperature and Peroxide Concentration. *J. Polym. Eng.* **2014**, *34* (7), 617–624. https://doi.org/10.1515/polyeng-2014-0034.

(7) Ferry, J. D. *Viscoelastic Properties of Polymers*; John Wiley & Sons, 1980.

(8) Wang, Z. Research on Fatigue Failure Mode and Failure Theory of Rubber. *J. Phys. Conf. Ser.* **2021**, *2076* (1), 012079. https://doi.org/10.1088/1742-6596/2076/1/012079.

(9) Physical, Thermal, and Mechanical Properties of Polymers. In *Biosurfaces*; John Wiley & Sons, Ltd, 2014; pp 329–344. https://doi.org/10.1002/9781118950623.app1.

(10) Hamed, G. R. Reinforcement of Rubber. *Rubber Chem. Technol.* **2000**, *73* (3), 524–533. https://doi.org/10.5254/1.3547603.

(11) Cañavate, J.; Colom, X.; Saeb, M. R.; Przybysz, M.; Zedler, L.; Formela, K. Influence of Microwave Treatment Conditions of GTR on Physico-Mechanical and Structural Properties of NBR/NR/GTR Composites. *Afinidad J. Chem. Eng. Theor. Appl. Chem.* **2019**, *76* (587).

(12) Brüning, K.; Schneider, K.; Roth, S. V.; Heinrich, G. Kinetics of Strain-Induced Crystallization in Natural Rubber Studied by WAXD: Dynamic and Impact Tensile Experiments. *Macromolecules* **2012**, *45* (19), 7914–7919. https://doi.org/10.1021/ma3011476.

(13) Brüning, K.; Schneider, K.; Roth, S. V.; Heinrich, G. Kinetics of Strain-Induced Crystallization in Natural Rubber Studied by WAXD: Dynamic and Impact Tensile Experiments. *Macromolecules* **2012**, *45* (19), 7914–7919. https://doi.org/10.1021/ma3011476.

(14) The Rubber Elastic State. In *Physical Properties of Polymers*; Samulski, E., Wignall, G., Koenig, J., Mark, J., Ngai, K., Mandelkern, L., Graessley, W., Eds.; Cambridge University Press: Cambridge, 2004; pp 3–71. https://doi.org/10.1017/CBO9781139165167.002.

(15) Vieyres, A.; Pérez-Aparicio, R.; Albouy, P.-A.; Sanseau, O.; Saalwächter, K.; Long, D. R.; Sotta, P. Sulfur-Cured Natural Rubber Elastomer Networks: Correlating Cross-Link Density, Chain Orientation, and Mechanical Response by Combined Techniques. *Macromolecules* **2013**, *46* (3), 889–899. https://doi.org/10.1021/ma302563z.

(16) Candau, N.; Laghmach, R.; Chazeau, L.; Chenal, J.-M.; Gauthier, C.; Biben, T.; Munch, E. Strain-Induced Crystallization of Natural Rubber and Cross-Link Densities Heterogeneities. *Macromolecules* **2014**, *47* (16), 5815–5824. https://doi.org/10.1021/ma5006843.

(17) Toki, S. The Effect of Strain-Induced Crystallization (SIC) on the Physical Properties of Natural Rubber (NR). In *Chemistry, Manufacture and Applications of Natural Rubber*; 2014; pp 135–167. https://doi.org/10.1533/9780857096913.1.135.

(18) Tosaka, M.; Murakami, S.; Poompradub, S.; Kohjiya, S.; Ikeda, Y.; Toki, S.; Sics, I.; Hsiao, B. S. Orientation and Crystallization of Natural Rubber Network As Revealed by WAXD Using Synchrotron Radiation. *Macromolecules* **2004**, *37* (9), 3299–3309. https://doi.org/10.1021/ma0355608.

(19) Albouy, P.-A.; Sotta, P. Strain-Induced Crystallization in Natural Rubber. In *Polymer Crystallization II*; Springer, Cham, 2015; pp 167–205. https://doi.org/10.1007/12_2015_328.

(20) Trabelsi, S.; Albouy, P.-A.; Rault, J. Effective Local Deformation in Stretched Filled Rubber. *Macromolecules* **2003**, *36* (24), 9093–9099. https://doi.org/10.1021/ma0303566.

(21) Sharma, R.; Bisen, D. P.; Shukla, U.; Sharma, B. G. X-Ray Diffraction: A Powerful Method of Characterizing Nanomaterials. *Recent Res. Sci. Technol.* **2012**.

(22) Huneau, B. STRAIN-INDUCED CRYSTALLIZATION OF NATURAL RUBBER: A REVIEW OF X-RAY DIFFRACTION INVESTIGATIONS. *Rubber Chem. Technol.* **2011**, *84* (3), 425–452. https://doi.org/10.5254/1.3601131.

(23) Cornelius, T. W.; Thomas, O. Progress of *in Situ* Synchrotron X-Ray Diffraction Studies on the Mechanical Behavior of Materials at Small Scales. *Prog. Mater. Sci.* **2018**, *94*, 384–434. https://doi.org/10.1016/j.pmatsci.2018.01.004.

(24) Yoshida, Y. Elastocaloric Effect on Natural Rubber and Terpolymer : Temperature Variation Mechanism, Morphology and Energy Balance during Deformation. phdthesis, Université de Lyon, 2016. https://theses.hal.science/tel-01695532 (accessed 2024-06-02).

(25) Mrad, M.; El Samra, R. Waste Tire Management: Lebanon Case Study. **2020**.

(26) Fazli, A.; Rodrigue, D. Recycling Waste Tires into Ground Tire Rubber (GTR)/Rubber Compounds: A Review. *J. Compos. Sci.* **2020**, *4* (3), 103. https://doi.org/10.3390/jcs4030103.

(27) Singh, S.; Nimmo, W.; Gibbs, B. M.; Williams, P. T. Waste Tyre Rubber as a Secondary Fuel for Power Plants. *Fuel* **2009**, *88* (12), 2473–2480.

(28) Aoudia, K.; Azem, S.; Aït Hocine, N.; Gratton, M.; Pettarin, V.; Seghar, S. Recycling of Waste Tire Rubber: Microwave Devulcanization and Incorporation in a Thermoset Resin. *Waste Manag.* **2017**, *60*, 471–481. https://doi.org/10.1016/j.wasman.2016.10.051.

(29) Dorigato, A.; Rigotti, D.; Fredi, G. Recent Advances in the Devulcanization Technologies of Industrially Relevant Sulfur-Vulcanized Elastomers. *Adv. Ind. Eng. Polym. Res.* **2023**, *6* (3), 288–309. https://doi.org/10.1016/j.aiepr.2022.11.003.

(30) Wiśniewska, P.; Wang, S.; Formela, K. Waste Tire Rubber Devulcanization Technologies: State-of-the-Art, Limitations and Future Perspectives. *Waste Manag.* **2022**, *150*, 174–184. https://doi.org/10.1016/j.wasman.2022.07.002.

(31) Scuracchio, C.; Waki, D.; Silva, M. Thermalanalysis of Ground Tire Rubber Devulcanized by Microwaves. *J. Therm. Anal. Calorim. - J THERM ANAL CALORIM* **2007**, *87*, 893–897. https://doi.org/10.1007/s10973-005-7419-8.

(32) Poyraz, S.; Liu, Z.; Liu, Y.; Zhang, X. Devulcanization of Scrap Ground Tire Rubber and Successive Carbon Nanotube Growth by Microwave Irradiation. *Curr. Org. Chem. 17* (20), 2243–2248.

(33) Shahamatifard, F.; Rodrigue, D.; Mighri, F. Thermal and Mechanical Properties of Carbon-Based Rubber Nanocomposites: A Review. *Plast. Rubber Compos.* **2023**, *52* (9–10), 483–505. https://doi.org/10.1080/14658011.2023.2231286.

(34) Song, J.; Tian, K.; Ma, L.; Li, W.; Yao, S. The Effect of Carbon Black Morphology to the Thermal Conductivity of Natural Rubber Composites. *Int. J. Heat Mass Transf.* **2019**, *137*, 184–191. https://doi.org/10.1016/j.ijheatmasstransfer.2019.03.078.

(35) Dwivedi, C.; Manjare, S.; Rajan, S. K. Recycling of Waste Tire by Pyrolysis to Recover Carbon Black: Alternative & Environment-Friendly Reinforcing Filler for Natural Rubber Compounds. *Compos. Part B Eng.* **2020**, *200*, 108346. https://doi.org/10.1016/j.compositesb.2020.108346.

(36) Song, J.; Li, X.; Tian, K.; Ma, L.; Li, W.; Yao, S. Thermal Conductivity of Natural Rubber Nanocomposites with Hybrid Fillers. *Chin. J. Chem. Eng.* **2019**, *27* (4), 928–934. https://doi.org/10.1016/j.cjche.2018.09.019.

(37) Valentín, J. L.; Carretero-González, J.; Mora-Barrantes, I.; Chassé, W.; Saalwächter, K. Uncertainties in the Determination of Cross-Link Density by Equilibrium Swelling Experiments in Natural Rubber. *Macromolecules* **2008**, *41* (13), 4717–4729. https://doi.org/10.1021/ma8005087.

(38) Guth, E. Theory of Filler Reinforcement. *J. Appl. Phys.* **1945**, *16* (1), 20–25. https://doi.org/10.1063/1.1707495.

(39) Trabelsi, S.; Albouy, P.-A.; Rault, J. Crystallization and Melting Processes in Vulcanized Stretched Natural Rubber. *Macromolecules* **2003**, *36* (20), 7624–7639. https://doi.org/10.1021/ma030224c.

(40) Candau, N.; Oguz, O.; Federico, C. E.; Stoclet, G.; Tahon, J.-F.; Maspoch, M. L. Strain Induced Crystallization in Vulcanized Natural Rubber Containing Ground Tire Rubber Particles with Reinforcement and Nucleation Abilities. *Polym. Test.* **2021**, *101*, 107313. https://doi.org/10.1016/j.polymertesting.2021.107313.

(41) Rault, J.; Marchal, J.; Judeinstein, P.; Albouy, P. A. Stress-Induced Crystallization and Reinforcement in Filled Natural Rubbers: 2H NMR Study. *Macromolecules* **2006**, *39* (24), 8356–8368. https://doi.org/10.1021/ma0608424.

(42) Candau, N.; Vives, E.; Fernández, A. I.; Maspoch, M. L. Elastocaloric Effect in Vulcanized Natural Rubber and Natural/Wastes Rubber Blends. *Polymer* **2021**, *236*, 124309. https://doi.org/10.1016/j.polymer.2021.124309.

(43) Wood, L. A.; Bekkedahl, N. Specific Heat of Natural Rubber and Other Elastomers Aboved the Glass Transition Temperature. *J. Polym. Sci. [B]* **1967**, *5* (2), 169–175. https://doi.org/10.1002/pol.1967.110050208.